Journal of Hydrology 636 (2024) 131262

Contents lists available at ScienceDirect

Journal of Hydrology

journal homepage: www.elsevier.com/locate/jhydrol

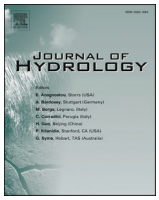

Research papers

Comparing sensitivities of groundwater head to variations in hydraulic parameters under boundary conditions of river stage rise and tidal variation

Jiong Zhu [a], Yuanyuan Zha [a,*], Tian-Chyi Jim Yeh [b], Walter A. Illman [c]

[a] State Key Laboratory of Water Resources Engineering and Management, Wuhan University, Wuhan 430072, China
[b] Department of Hydrology and Atmospheric Sciences, University of Arizona, Tucson, AZ 85721, USA
[c] Department of Earth and Environmental Sciences, University of Waterloo, Waterloo, Ontario N2L3G1, Canada

ARTICLE INFO

This manuscript was handled by Yuefei Huang, Editor-in-Chief, with the assistance of Jian Luo, Associate Editor

Keywords:
Sensitivity
Sensitivity equation method
Fréchet kernels
Head responses
Tidal variation

ABSTRACT

The sensitivity of hydraulic head responses to spatially distributed hydraulic parameters is essential for uncertainty analysis, inverse modeling, and parameter estimation and interpretation. This study formulates the Fréchet sensitivity kernel of hydraulic head responses to a suddenly rising boundary and a sinusoidal head fluctuation boundary to variation of spatially distributed hydraulic parameters in a semi-infinite, one-dimensional (1-D), confined aquifer, and it then derives analytical solutions. Different from previous studies that derived expressions for Fréchet kernels in the time domain for a 2-D pumping test, this study is the first to derive the closed-form Fréchet kernels in time and frequency domains for a semi-infinite, 1-D, confined aquifer. This study uses the Fréchet kernels to investigate the nature of singularities in the spatial sensitivity functions around the observation location and boundary. The information content revealed by observation of head change or head fluctuation amplitude at a given specified location and time (or frequency) under the above two boundary conditions is different. When comparing Fréchet sensitivity kernels across various times or periods, multi-frequency information, much like multi-time information, can be instrumental for hydrogeological parameter inversion. The explicit-form Fréchet sensitivity kernels also identify the optimal time or period for obtaining measurements.

1. Introduction

Sensitivity analysis explores the response of model output to the change of its inputs. Sensitivity coefficients can reveal model characteristics (such as aquifer heterogeneity (Huang and Yeh, 2007; Leven and Dietrich, 2006)) and provide a better understanding of the system and its behaviors. Sensitivity analysis also plays a vital role in inverse problems (Kitanidis and Vomvoris, 1983; Yeh, 1986), such as selecting the most effective observation information and its sampling locations, types, and optimum times (Mao et al., 2013; Pechstein et al., 2015; Sun et al., 2013; Yeh and Liu, 2000; Zha et al., 2014). Sensitivity analysis has been used successfully in a variety of groundwater flow applications (e.g., the design of optimal pumping and injection schemes and the estimation of aquifer parameters from monitoring data) (Copty et al., 2011; Manewell et al., 2023; Mclaughlin et al., 1996; Pechstein et al., 2015).

Aquifer characterization is essential to accurately predict and monitor the migration of groundwater contaminants (Dagan, 1982b,a). Accurate delineation of local groundwater flow directions and hydraulic gradients is difficult unless the spatial distribution of aquifer parameters, such as transmissivity T, and storativity S, could be characterized in detail (Carrera and Neuman, 1986; Clifton and Neuman, 1982; Kitanidis, 1995; Kitanidis and Vomvoris, 1983). In many cases (Pouladi et al., 2021; Shuai et al., 2017; Sobolevskaia et al., 2021), S was considered uniform and attention had been focused on the spatial variability of diffusivity (D, the ratio of transmissivity T to storativity S). This problem is especially important if the two parameters are correlated as estimated values of T and S are expected to be disproportionately sensitive to groundwater flow. Therefore, the joint estimation of T and S is needed (Castagna et al., 2011; Zhao and Illman, 2021).

To capture the complex distribution of aquifer properties, hydraulic tomography (HT), to collect non-redundant drawdown data by switching pumping locations in the aquifer has been proposed by Yeh and Liu, (2000), and the data are subsequently interpreted using an adjoint state method to construct sensitivity and stochastic cross-correlation relationships to map a heterogeneous medium. Following the tomographic survey concepts, Sun et al. (2013), Zha et al. (2014), and Xia et al. (2023) mapped the aquifer properties by its head responses to river-stage rises or pumping test under different temporal sampling to

* Corresponding author.
E-mail address: zhayuan87@whu.edu.cn (Y. Zha).

https://doi.org/10.1016/j.jhydrol.2024.131262
Received 10 November 2023; Received in revised form 21 March 2024; Accepted 13 April 2024
Available online 30 April 2024

characterize heterogeneous aquifers under the influence of reservoir impoundment, river channels or pumping.

Recently, a method for determining the hydrogeological parameters of aquifers, based on head propagation due to tidal variations has been proposed (Erskine, 1991; Fischer et al., 2020; Trefry et al., 2011; Trefry and Bekele, 2004; Zhang, 2021). In these studies, the amplitude and the phase shift of the observed steady-periodic signals at the observation wells were used to reveal the spatial structure of aquifer properties (Shuai et al., 2017; Sobolevskaia et al., 2021). Unlike the head response to river stage rise, the fluctuations of hydraulic heads in response to tidal variations are quasi-steady, with a fixed frequency equal to the tidal boundary (Mohri et al., 2010). However, head response to tidal variation and river stage rise shows common characteristics: for example, the amplitude of tidal variation decays along the distance, similar to the propagation of hydraulic head caused by a river stage rise (Vandenbohede and Lebbe, 2007). Moreover, the periodicities (frequency) of the tidal responses at different distances are analogous to arrival times of head propagation (Hwang et al., 2020; Johnson et al., 2012; Qi et al., 2022; Wang et al., 2019). The arrival time of the head propagation in aquifers is generally fast near the river bank, corresponding to a high-frequency fluctuating signal of tidal variation (Rowe, 1960; Trefry, 1999).

HT relies on a highly parameterized geostatistical inverse model, where the calculation of sensitivity maps plays a crucial role (Zha et al., 2020). Sensitivity maps, or more formally Fréchet sensitivity kernel (Oliver, 1993), measure the sensitivity of a single hydraulic head observation to all independent spatial parameters within the area of interest (Mazzilli et al., 2010). Fréchet kernel determines the effective "volume of influence" or "spatial weighting functions" that a perturbation expansion causes the resultant small change in the measured output under the assumption that the hydraulic parameter is spatially uniform (Knight and Kluitenberg, 2005). Fréchet kernels can be equivalent to sensitivity analysis, showing that a travel time measurement has the sensitivity to aquifer parameters everywhere along a ray path. Based on sensitivity analysis, the most effective observation information, such as sampling locations (Slooten et al., 2010), types (Zha et al., 2014), and optimal times (Sun et al., 2013) can be selected in geostatistical inversion. Optimal test design could be achieved from the Fréchet sensitivity kernel whereby, for instance, increased input measurements and sampling at points of maximum sensitivity improve the accuracy of aquifers' estimated parameters. As such, the computation of the Fréchet sensitivity kernel stands as a preliminary yet a crucial step in geostatistical inversion, geared towards a thorough understanding of aquifer heterogeneity (Leven and Dietrich, 2006).

Additionally, Fréchet kernels are used to interpret and estimate spatially averaged transmissivities for the case of single-well pumping tests. For example, Copty et al. (2011) developed a Continuous-Derivation method to yield time-dependent transmissivity from constant-flow pumping tests in heterogeneous and confined aquifers and interpreted transient drawdown data by Fréchet kernels. Pechstein et al. (2015) used Fréchet kernels and the time-derivative of the Fréchet kernel to obtain estimates of representative flow parameters.

Typically, the Fréchet sensitivity kernel can be obtained numerically using the perturbation, adjoint state, and sensitivity equation methods. The benefits and challenges of each method have been extensively dissected in prior research (Knight and Kluitenberg, 2005; Leven and Dietrich, 2006; Lu and Vesselinov, 2015; Zha et al., 2020).

Time series of groundwater head induced by boundary forcing in a semi-infinite, 1-D, confined aquifer can be decomposed into two types of fundamental signals: head rise signal induced by a sudden rising boundary head (Heaviside function), and head variation signal induced by a sinusoidal head fluctuation of a specific frequency at a boundary. These two fundamental signals, from temporal and frequency-domain perspectives, respectively, can thus recover the original time series via temporal convolution or superposition. This paper aims to derive the Fréchet sensitivity kernels for a 1-D semi-infinite confined aquifer due to sudden rising boundary head and tidal variation signal via the sensitivity equation based on the work of Zha et al. (2020).

Unlike previous studies of Fréchet kernels in the time domain for 2-D pumping test problems, this study derives the Fréchet kernels for a 1-D semi-infinite aquifer to characterize aquifers under the reservoir impoundment and river channels. It further derives explicit-form Fréchet kernels in the frequency domain for the first time, which is significant in characterizing coastal aquifers. The explicit-form Fréchet kernels yield considerable insight into the properties. Ultimately, our analyses of Fréchet sensitivity kernels can facilitate a swift and straightforward interpretation of hydraulic and geophysical inversion problems, contributing valuable insights to both fields.

2. Statement of the problem

2.1. Governing equations and related analytical solutions

Case 1: Sudden rise of the river stage

The propagation of groundwater hydraulic head induced by a sudden rising boundary in a semi-infinite, confined, 1-D heterogeneous aquifer can be quantified by the following equation:

$$\frac{\partial}{\partial x}\left[T(x)\frac{\partial H(x,t)}{\partial x}\right]=S(x)\frac{\partial H(x,t)}{\partial t} \tag{1}$$

where t [T] represents time and x [L] denotes the horizontal coordinate. $S(x)$[dimensionless] and $T(x)$ [L^2/T] represent the spatially-varying storativity and transmissivity parameters, respectively. $H(x,t)$, [L], is the hydraulic head at x and t. Additionally, the initial and boundary conditions for this situation are:

$$H(x,t)=H_0,\quad t=0 \tag{2.a}$$

$$H(0,t)=H_0+H_s \tag{2.b}$$

$$H(\infty,t)=H_0,\quad x\to\infty \tag{2.c}$$

where H_0 [L] denotes the initial constant groundwater head over the aquifer, while H_s [L] represents the elevation of the river stage rise at the boundary ($x=0$) at $t=0$, representing a Dirichlet boundary condition. The rising river stage boundary is assumed to rise at $t=0$ and remains constant over time.

If the boundary is a Neumann boundary condition with a fixed flux, q [L^2/T], Eq. (2.b) is replaced by:

$$T\frac{\partial H(0,t)}{\partial x}\bigg|_{x=0}=q \tag{2.d}$$

In the case that storativity and transmissivity are spatially uniform with values T and S, the head solution (excluding the constant groundwater level H_0) for Eqs. (2.a)–(2.c) (Welch et al., 2013) is:

$$H(x,t)=H_s erfc\left(\frac{x}{2\sqrt{Dt}}\right) \tag{3}$$

where $erfc(.)$ is complementary error function, and $erfc(z)=\frac{2}{\sqrt{\pi}}\int_0^z e^{-u^2}du$. D [L^2/T] is the aquifer diffusivity (equal to T/S). Letting $\frac{1}{2\sqrt{Dt}}=a_1$ [L^{-1}], we have $H(x,t)=H_s erfc(a_1 x)$.

If the Neumann boundary condition (Eq. (2.d)) is considered, the solution to Eq. (1) is:

$$H(x,t)=-\frac{q}{a_1 T}ierfc(a_1 x) \tag{4}$$

where $ierfc(.)$ is the integral of the complementary error function, and $ierfc(z)=\int_{-\infty}^{z}erfc(u)du=\frac{1}{\sqrt{\pi}}exp(-z^2)-zerfc(z)$.

Case 2: Tidal variation of the river stage

Instead of a sudden rise at a constant head at $x = 0$ and $t = 0$, we now consider the variation as a periodic cosine function in time, representing tidal fluctuations. Using Euler's formula, we represent the H_s as the real part of a complex expression, and at $x = 0$, Eq. (2. a) is written as:

$$H = H_0 + H_s cos(\omega t + \varphi) = H_0 + Re(H_s e^{i\omega t}) \tag{5}$$

where $i = \sqrt{-1}$ is an imaginary number, ω [T^{-1}] is angle frequency, φ [dimensionless] is the phase angle, and $Re(.)$ represents the real part of a complex expression. Assuming t_p [T] is the period, we have $t_p = \frac{2\pi}{\omega}$. Furthermore, we assume that the head fluctuation has reached a steady state with the frequency ω [T^{-1}] (Guo et al., 2010; Guo et al., 2007; Li et al., 2006; Trefry and Johnton, 1998).

In this case, the head response can be expressed in a complex form: $H(x,t) = H_0 + Re(G(x,\omega)e^{i\omega t})$, where $G(x,\omega)$ is the complex frequency response function for the aquifer. The amplitude of the head oscillation at location x is $A_G = \left|G(x,\omega)e^{i\omega t}\right|$ [L], and the phase shift between the head at the tidal boundary and the location x is, $P_G = arg\{G(x,\omega)e^{i\omega t}\} - arg\{H_s e^{i\omega t}\}$ [dimensionless]. By utilizing the complex expressions of $H(x,t)$ in Eq. (1) and its boundary conditions Eq. (2), we obtain a 1-D governing equation for flow in the heterogeneous aquifer under steady periodic oscillation,

$$\frac{\partial}{\partial x}\left[T(x)\frac{\partial G(x,\omega)}{\partial x}\right] = S(x)i\omega G(x,\omega) \tag{6}$$

$$G(x,\omega) = H_s, \quad x \to 0 \tag{7.a}$$

$$G(x,\omega) = 0, \quad x \to \infty \tag{7.b}$$

Likewise, analytical solutions for heterogeneous aquifers do not exist except for a spatially uniform case with values T and S (Sobolevskaia et al., 2021):

$$G(x,\omega) = H_s exp\left(-\sqrt{\frac{i\omega}{D}}x\right) \tag{8}$$

Letting $\sqrt{\frac{\omega S}{2T}} = a_2[L^{-1}]$, we have $G(x,\omega) = H_s exp(-a_2 x) exp(-a_2 x i)$, and substituting it into $H(x,t) = H_0 + Re(G(x,\omega)e^{i\omega t})$, we obtain:

$$H(x,t) = H_0 + H_s exp(-a_2 x) cos(\omega t - a_2 x) \tag{9}$$

Eq. (9) shows that the amplitude and phase shift at location x are $A_G = H_s exp(-a_2 x)$ and $P_G = arctan(-a_2 x)$, respectively.

2.2. Sensitivities and Fréchet kernels

It is easy to show the connection between traditional sensitivities and Fréchet kernels. We compare the Fréchet kernels with the following numerical solutions. We define the traditional sensitivities $I \approx \frac{\partial u}{\partial x_j}$, which is the effect of x perturbation in the subdomain x_j on an observation u (hydraulic head, amplitude, and phase shift). Many studies (Copty et al., 2011; Knight and Kluitenberg, 2005) have indicated that the sensitivity coefficient I is equal to the spatial integrals over the subdomain region of the corresponding spatial sensitivity functions (Fréchet kernel, F), i.e.,

$$I = \int_{x_j} F dx \tag{10}$$

2.3. Dimensionless variables

All results of this study are expressed in terms of dimensionless variables such that they are scalable. Specifically, the head or fluctuation observation distance x_o and dimensionless observation distance x_o^*, the perturbation parameter distance x_Y and the dimensionless parameter distance x_Y^*, the frequency ω and the dimensionless frequency ω^*, and the time t and the dimensionless time t^* are converted as follows:

$$\begin{cases} x_Y^* = \frac{x_Y}{x_o} \\ x_o^* = \frac{x_o}{x_o} = 1 \\ t^* = \frac{Tt}{Sx_o^2} \\ \omega^* = \sqrt{\frac{\omega S}{T}}x_o \end{cases} \tag{11}$$

3. Sensitivities of head or fluctuation change to homogeneous T or S

This section examines the sensitivities of the hydraulic head or fluctuation in a homogeneous aquifer using the simple derivation method of the above two cases.

We define the total sensitivities I_{tot} as the sensitivity of H or A_G/P_G at location x_o at a given time t or frequency ω to change in T and S values of the homogeneous aquifer. According to Eq. (3) and Eq. (8), we can easily obtain:

$$I_{HS,tot} = \frac{dH(x_o,t)}{dS} = -\frac{H_s x_o exp(-x_o{}^2 S/4tT)}{2\sqrt{\pi}S\sqrt{tT/S}} \tag{12.a}$$

$$I_{HT,tot} = \frac{dH(x_o,t)}{dT} = \frac{H_s x_o exp(-x_o{}^2 S/4tT)}{2\sqrt{\pi}T\sqrt{tT/S}} \tag{12.b}$$

$$I_{AS,tot} = \frac{dA_G(x_o,\omega)}{dS} = -\frac{H_s x_o \sqrt{\frac{S\omega}{T}} exp(-x_o\sqrt{\frac{S\omega}{2T}})}{2\sqrt{2}S} \tag{12.c}$$

$$I_{AT,tot} = \frac{dA_G(x_o,\omega)}{dT} = \frac{H_s x_o \sqrt{\frac{S\omega}{T}} exp(-x_o\sqrt{\frac{S\omega}{2T}})}{2\sqrt{2}T} \tag{12.d}$$

$$I_{PS,tot} = \frac{dP_G(x_o,\omega)}{dS} = -\frac{x_o\omega}{\sqrt{\frac{2S\omega}{T}}(2T + S\omega x_o{}^2)} \tag{12.e}$$

$$I_{PT,tot} = \frac{dP_G(x_o,\omega)}{dT} = \frac{x_o\sqrt{\frac{S\omega}{T}}}{\sqrt{2}(2T + S\omega x_o{}^2)} \tag{12.f}$$

where $I_{HS,tot}$ [L], $I_{HT,tot}$ [L^{-1} T], $I_{AS,tot}$ [L], $I_{AT,tot}$ [L^{-1} T], $I_{PS,tot}$ [dimensionless] and $I_{PT,tot}$ [L^{-2} T] represent the total traditional sensitivity coefficient of the hydraulic head, amplitude, and phase shift at the observation point to storativity and transmissivity throughout the domain, respectively.

The dimensionless forms of the total sensitivities I_{tot} (Eqs. (12.a)–(12.f)), are:

$$I_{HS,tot}{}^* = \frac{S}{H_s}I_{HS,tot} = -\frac{exp(-1/4t^*)}{2\sqrt{\pi t^*}} \tag{13.a}$$

$$I_{HT,tot}{}^* = \frac{T}{H_s}I_{HT,tot} = \frac{exp(-1/4t^*)}{2\sqrt{\pi t^*}} \tag{13.b}$$

$$I_{AS,tot}{}^* = \frac{S}{H_s}I_{AS,tot} = -\frac{\omega^* exp(-\omega^*/\sqrt{2})}{2\sqrt{2}} \tag{13.c}$$

$$I_{AT,tot}{}^* = \frac{T}{H_s}I_{AT,tot} = \frac{\omega^* exp(-\omega^*/\sqrt{2})}{2\sqrt{2}} \tag{13.d}$$

$$I_{PS,tot}{}^* = SI_{PS,tot} = -\frac{\omega^*}{\sqrt{2}(2+\omega^{*2})} \tag{13.e}$$

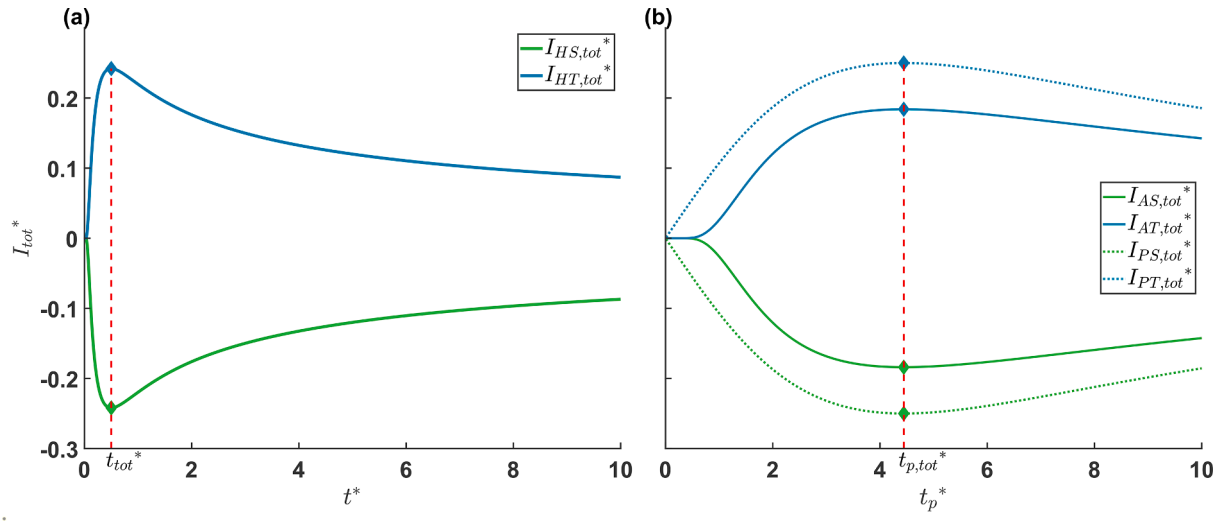

Fig.1. (a) Dimensionless head total sensitivity coefficient to storativity, $I_{HS,tot}{}^*$, and total sensitivity coefficient to transmissivity, $I_{HT,tot}{}^*$, as a function of dimensionless time t^*. (b) Dimensionless total amplitude sensitivity coefficient to storativity, $I_{AS,tot}{}^*$, total amplitude sensitivity coefficient to transmissivity, $I_{AT,tot}{}^*$, total phase shift sensitivity coefficient to storativity, $I_{PS,tot}{}^*$, and total phase shift sensitivity coefficient to transmissivity, $I_{PT,tot}{}^*$ as a function of dimensionless period $t_p{}^*$ for the tidal case.

$$I_{PT,tot}{}^* = TI_{PT,tot} = \frac{\omega^*}{\sqrt{2}(2+\omega^{*2})} \tag{13.f}$$

It must be emphasized that the dimensionless total sensitivity coefficients, $I_{tot}{}^*$, depend on the distance of the observation point from the boundary, although this is not explicit in the forms of (Eqs. (13.a)–(13.f)), as they are only functions of dimensionless variables t^* or ω^*.

Fig. 1(a) shows the dimensionless head sensitivities to storativity ($I_{HS,tot}{}^*$) and transmissivity ($I_{HT,tot}{}^*$) as a function of dimensionless time t^*. The tidal response's dimensionless amplitude sensitivities to storativity, $I_{AS,tot}{}^*$, and transmissivity, $I_{AT,tot}{}^*$ are illustrated in Fig. 1(b), which also displays the phase shift sensitivities to storativity ($I_{PS,tot}{}^*$) and transmissivity ($I_{PT,tot}{}^*$) as a function of the dimensionless period $t_p{}^*$ (dimensionless period and $t_p{}^* = \frac{2\pi}{\omega^*}$).

According to Figs. 1(a) and (b), the sensitivities to T and S have the same patterns, but opposite signs for the homogeneous aquifer. For the sudden rising boundary, $I_{HT,tot}{}^*$ is always positive and reaches the highest peak value at the time $t_{tot}{}^* = 0.5$, when $I_{HS,tot}{}^*$ reaches negative maximum. The results are different from a pumping test in a 2-D domain for the homogeneous aquifer. At early times the head at the observation well is positively correlated with T. It becomes negatively correlated later, and at the intermediate time when the sensitivity of H and T is zero, the sensitivity of the H and S reaches a negative maximum (see Fig. 1(a) in Sun et al., 2013).

Similar to the tidal response in Fig. 1(b), amplitude sensitivities and phase shift sensitivities have the same patterns as head sensitivities and reach the highest peak value at the period $t_{p,tot}{}^* \approx 4.44$. These results suggest that signals at the observation location due to the excitation from the rise of the river stage or tidal oscillation carry the same information about T and S of an aquifer.

4. Deriving the Fréchet kernel via the sensitivity equation

This section examines the Fréchet sensitivity kernels of the hydraulic head or fluctuation at a given location as a function of time or frequency to unknown parameter values in a heterogeneous aquifer, using sensitivity equations for the above two cases.

In the following context, we assume that the $T(x)$ and $S(x)$ in the aquifer are stochastic fields characterized by ensemble statistics (means and covariances). They satisfy the stationary assumption in geostatistical theory with spatially uniform means with random local variations. These mean values are denoted as $\langle T\rangle$ and $\langle S\rangle$. Consequently, the derivatives of the Fréchet sensitivity kernels are assessed at the ensemble mean parameter values rather than specific realizations of the random field. The resulting sensitivities are the ensemble mean sensitivities, which could be used to evaluate the cross-covariance behaviors between the head and parameter perturbations. Besides, this approach allows us to derive an explicit-form Fréchet kernel since it is calculated as the integration of head or fluctuation solution (governed by groundwater flow equation Eq. (3) or (8)) and sensitivity equation (governed by sensitivity equation, Eq. (14) or (16)), the closed forms that only exist for ensemble homogeneous cases.

The aquifers considered are heterogeneous, but the Fréchet kernels approach assumes the aquifers are homogeneous in the ensemble mean. It yields sensitivities different from those in a spatially homogeneous aquifer in Section 3. The approximation embedded in Fréchet kernels is restricted to scenarios with small-variance heterogeneity.

4.1. Sensitivity equations for heterogeneous T and S fields

Case 1: River stage rise as a time function

Suppose we are interested in the sensitivity of hydraulic head $H(x_o,t)$ at the location x_o and time t, induced by river stage rises, to a change in the parameter Y (i.e., T or S) at the location x_Y in a heterogeneous aquifer. Defining $\phi_H(x_o,t;x_Y) = \partial H(x_o,t)/\partial Y(x_Y)$, and differentiating Eq. (1) with respect to Y, we have the sensitivity equation:

$$\frac{\partial}{\partial x}\left[T(x)\frac{\partial \phi_H(x,t)}{\partial x} + \frac{\partial T(x)}{\partial Y(x_Y)}\frac{\partial H(x,t)}{\partial x}\right] = S(x)\frac{\partial \phi_H(x,t)}{\partial t} + \frac{\partial H(x,t)}{\partial t}\frac{\partial S(x)}{\partial Y(x_Y)} \tag{14}$$

The associated initial and boundary conditions for the sensitivity equation are

$$\phi_H(x,t) = 0,\ \ t = 0 \tag{15.a}$$

$$\phi_H(x,t) = 0,\ \ |x - x_Y| \to \infty \tag{15.b}$$

Of course, one must solve Eq. (1) for $H(x,t)$ with given $T(x)$ and $S(x)$ fields and initial and boundary conditions for the flow. $H(x,t)$ then is used in Eq. (14).

Case 2: Tidal variation as a frequency function

Next, we examine the sensitivity equation of the complex frequency head response, G (x_o, ω), at the location x_o, induced by the tidal variation, to a change in the parameter Y at the location x_Y in a heterogeneous aquifer. Denoting the sensitivity as $\phi_G(x_o, \omega; x_Y) = \partial G(x_o, \omega)/\partial Y(x_Y)$, and differentiating Eq. (6) with respect to Y, we have the sensitivity equation:

$$\frac{\partial}{\partial x}\left[T\frac{\partial \phi_G}{\partial x}+\frac{\partial T}{\partial Y(x_Y)}\frac{\partial G}{\partial x}\right]=i\omega S\phi_G+i\omega G\frac{\partial S}{\partial Y(x_Y)} \tag{16}$$

with the initial and boundary conditions:

$$\phi_G(x,\omega)=0,\ x\to 0 \tag{17.a}$$

$$\phi_G(x,\omega)=0,\ |x-x_Y|\to\infty \tag{17.b}$$

To solve the above sensitivity equations, we use the method of image wells (or the principle of superposition) since these equations involve the change of a parameter at a given location within the flow domain. The following sections illustrate the application of the method.

4.2. Sensitivity of H to S

In this case, we replace Y with S in Eq. (14) and assume that T and S are independent. Eq. (14) becomes:

$$\frac{\partial}{\partial x}\left[T(x)\frac{\partial \phi_H(x,t)}{\partial x}\right]-\frac{\partial H(x,t)}{\partial t}\delta(x-x_Y)=S(x)\frac{\partial \phi_H(x,t)}{\partial t} \tag{18}$$

Eq. (18) is the sensitivity equation for $\phi_H(x,t)$ that describes the impact of the change in S value at the location x_Y on the hydraulic head, $H(x,t)$, over the domain at all times. Notice that $\delta(x-x_Y)$ is a Dirac delta function that is zero everywhere except a single point $x=x_Y$ where it becomes infinity and it describes the effect of S perturbation on the result when we focus only on x_Y. Therefore, the second term on the left-hand side of the equation is the rate of change in the hydraulic head at that location. It is a time-varying excitation that drives the spatiotemporal variation of $\phi_H(x,t)$ with given initial and boundary conditions described by Eqs. (15. a) and (15. b). Again, $T(x)$ and $S(x)$ must be specified and the rate of change in the hydraulic head at location, x_Y, must be given.

Analytically solving the sensitivity equation (Eq. (18)) is out of the question. As a result, a temporal convolution (Duhamel's superposition integral) is used for the calculation of $\phi_H(x,t)$ based on the superposition principle (Zha et al., 2020). According to Duhamel's superposition integral, we can get $\phi_H(x,t)=\int_0^t \frac{\partial H(x,\tau)}{\partial \tau}\phi_0(x,t-\tau;x_Y)d\tau$, where $\phi_0(x,t;x_Y)$ is a fundamental solution describing the sensitivity of the hydraulic head by a unit impulse at time 0 and location x_Y. $\phi_0(x,t;x_Y)$ in a realization of heterogeneous S fields is governed by:

$$\frac{\partial}{\partial x}\left[T(x)\frac{\partial \phi_0}{\partial x}\right]+\delta(x-x_Y)\delta(t-0)=S(x)\frac{\partial \phi_0}{\partial t} \tag{19}$$

subject to the given initial and boundary conditions (i.e., Eqs. (15. a) and (15. b) with ϕ_H replaced by ϕ_0). Notice that the second term on the left-hand side of Eq. (19) exists only at $t=0$.

The detailed process of solving Eq. (19) by the method of image well is shown in Appendix A, where ϕ_0 is:

$$\phi_0(x,t;x_Y)=-\frac{1}{2T}\frac{\sqrt{D}}{\sqrt{\pi}}\left[exp\left(-\frac{|x_Y-x|^2}{4Dt}\right)t^{-1/2}-exp\left(-\frac{|x_Y+x|^2}{4Dt}\right)t^{-1/2}\right] \tag{20}$$

$\frac{\partial H}{\partial t}\big|_{x_Y}$ is given by Eq. (3):

$$\left.\frac{\partial H}{\partial t}\right|_{x_Y}=\frac{H_s x_Y}{2\sqrt{\pi D}}exp\left(-\frac{x_Y^2}{4Dt}\right)t^{-3/2} \tag{21}$$

Since the convolution can be solved conveniently by Laplace transform due to the fact that $\mathscr{L}\left[\int_0^t f(t-\tau)g(t)d\tau\right]=\mathscr{L}[f(t)]\mathscr{L}[g(t)]$, where $\mathscr{L}(.)$ is Laplace transform, we first obtain the Laplace transform of ϕ_H:

$$\mathscr{L}(\phi_H)=\mathscr{L}(\phi_0)\mathscr{L}\left(\left.\frac{\partial H}{\partial t}\right|_{x_Y}\right)$$

$$=-\frac{H_s\sqrt{D}}{2T\sqrt{p}}exp\left(-\sqrt{\frac{p}{D}}x_Y\right)\left[exp\left(-\sqrt{\frac{p}{D}}|x_Y-x|\right)-exp\left(-\sqrt{\frac{p}{D}}|x_Y+x|\right)\right] \tag{22}$$

where p [T^{-1}] is the Laplace transform parameter.

According to the inverse Laplace transform, we have

$$F_S=\phi_H(x_o,t;x_Y)$$

$$=-\frac{H_s\sqrt{D}}{2T\sqrt{\pi t}}\left[exp\left(-\frac{(x_Y+|x_Y-x_o|)^2}{4Dt}\right)-exp\left(-\frac{(x_Y+|x_Y+x_o|)^2}{4Dt}\right)\right] \tag{23}$$

where F_S [dimensionless] is the sensitivity of head response $H(x_o,t)$ on S, i.e., the Fréchet kernel of heterogeneous storativity on head response.

4.3. Sensitivity of H to T

Note that any function times the Dirac delta function (e.g., $f(x)\delta(x-x_c)$) will result in missing information of $f(x)$ except its value at point $x=x_c$. That is, $f(x)\delta(x-x_c)$ should be considered as $f(x_c)\delta(x-x_c)$ before it is applied with the outer partial derivative operator. Since $f(x_c)$ is a constant number, it can be directly taken out of the derivative. As a result, replacing Y with T at location x_Y, Eq. (14) can be rewritten as:

$$\frac{\partial}{\partial x}\left[T\frac{\partial \phi_H}{\partial x}\right]+\frac{\partial}{\partial x}\left[\delta(x-x_Y)\frac{\partial H}{\partial x}\right]=S\frac{\partial \phi_H}{\partial t} \tag{24}$$

The derivative of the Dirac delta function can be written in a limit form:

$$\frac{\partial}{\partial x}\left[T\frac{\partial \phi_H}{\partial x}\right]+\left.\frac{\partial H}{\partial x}\right|_{x_Y}\left[\frac{\partial \delta(x-x_Y)}{\partial x}\right]=S\frac{\partial \phi_H}{\partial t} \tag{25}$$

Referring to Eq. (19), the fundamental solution ϕ_{TH} of the equation is subjected to $\frac{\partial}{\partial x}\left[T\frac{\partial \phi_{TH}}{\partial x}\right]+\left[\frac{\partial \delta(x-x_Y)}{\partial x}\right]\delta(t-0)=S\frac{\partial \phi_{TH}}{\partial t}$, and the limit operators can be replaced by the partial derivative. Comparing Eq. (19) with this equation, we can get:

$$\mathscr{L}(\phi_{TH})=\frac{\partial \mathscr{L}(\phi_0)}{\partial x} \tag{26}$$

and $\frac{\partial H}{\partial x}\big|_{x_Y}$ is given by Eq. (3):

$$\left.\frac{\partial H}{\partial x}\right|_{x_Y}=-\frac{H_0}{\sqrt{\pi D t}}exp\left(-\frac{x_Y^2}{4Dt}\right) \tag{27}$$

Similar to Eq. (22), we can get:

$$\mathscr{L}(\phi_H)=\mathscr{L}(\phi_{TH})\mathscr{L}\left(\left.\frac{\partial H}{\partial x}\right|_{x_Y}\right)$$

$$= \begin{cases} \frac{H_0}{2T\sqrt{Dp}} exp\left(-\sqrt{\frac{p}{D}}x_Y\right)\left[exp\left(-\sqrt{\frac{p}{D}}(x-x_Y)\right)+exp\left(-\sqrt{\frac{p}{D}}(x_Y+x)\right)\right], & x_Y < x \\ \frac{H_0}{2T\sqrt{Dp}} exp\left(-\sqrt{\frac{p}{D}}x_Y\right)\left[-exp\left(-\sqrt{\frac{p}{D}}(x_Y-x)\right)+exp\left(-\sqrt{\frac{p}{D}}(x_Y+x)\right)\right], & x_Y > x \end{cases} \quad (28)$$

According to the inverse Laplace transform, we have

$$F_T = \phi_H(x_o, t; x_Y)$$

$$= \begin{cases} \frac{H_0}{2T\sqrt{D\pi t}}\left[exp\left(-\frac{(x_Y+|x_Y-x_o|)^2}{4Dt}\right)+exp\left(-\frac{(x_Y+|x_Y+x_o|)^2}{4Dt}\right)\right], & x_Y < x_o \\ \frac{H_0}{2T\sqrt{D\pi t}}\left[-exp\left(-\frac{(x_Y+|x_Y-x_o|)^2}{4Dt}\right)+exp\left(-\frac{(x_Y+|x_Y+x_o|)^2}{4Dt}\right)\right], & x_Y > x_o \end{cases} \quad (29)$$

where F_T [L^{-2} T] is the sensitivity of head response $H(x_o, t)$ on T, i.e., the Fréchet kernel of heterogeneous transmissivity on head response.

4.4. Sensitivity of G toS

To explore the sensitivity of tidal response on storativity, replacing Y to S at the location x_Y, Eq. (13) can be simplified as

$$\frac{\partial}{\partial x}\left[T\frac{\partial \phi_G}{\partial x}\right] - i\omega G(x_Y)\delta(x-x_Y) = i\omega S\phi_G \quad (30)$$

with the initial and boundary conditions $\phi_G(x,\omega) = 0, x \to 0$ and $\phi_G(x,\omega) = 0, |x - x_Y| \to \infty$.

First, we can consider a fundamental form of Eq. (30), similar to Eq. (19):

$$\frac{\partial}{\partial x}\left[T\frac{\partial \phi_g}{\partial x}\right] + \delta(x-x_Y) = i\omega S\phi_g \quad (31)$$

subject to the initial and boundary conditions $\phi_g(x,\omega) = 0, x \to 0$ and $\phi_g(x,\omega) = 0, |x - x_Y| \to \infty$. According to Eq. (8) and the method of image well in Appendix A, the fundamental solution of Eq. (31) is:

$$\phi_g = \sqrt{\frac{T}{i\omega S}}\frac{1}{2T}\left[exp\left(-\sqrt{\frac{i\omega S}{T}}|x_Y - x|\right) - exp\left(-\sqrt{\frac{i\omega S}{T}}|x_Y + x|\right)\right] \quad (32)$$

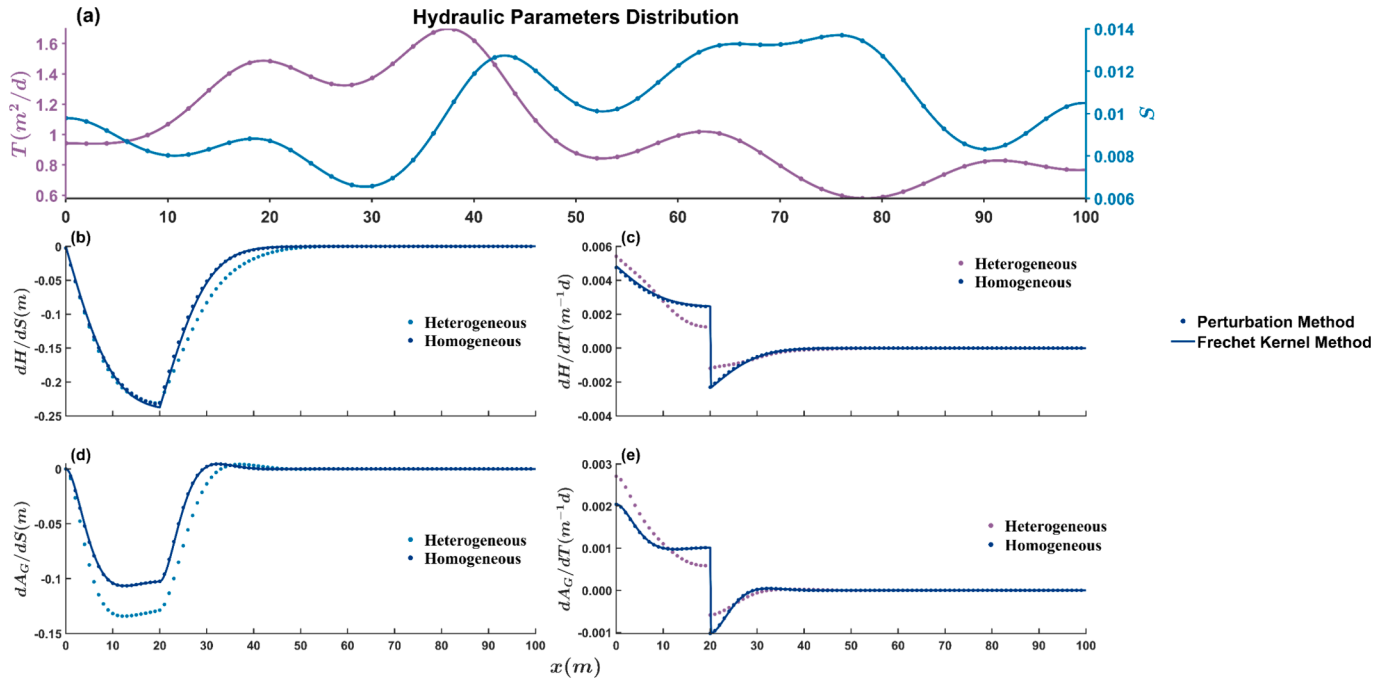

Fig. 2. (a) The T and S have a lognormal distribution with a correlation length of 30 m, where the means, μ, for T and S are 1 m^2/d and 0.01 and the standard deviations, σ, are 0.5 m^2/d and 0.005; Sensitivities of H at $x = 20m$ and $t = 2d$ to (b) S or (c) T calculated by perturbation (as the dots show) under heterogeneous parameters (Fig. 2(a)) or homogeneous parameters versus calculated by Fréchet kernels (as the lines show). Sensitivities of A_G at $x = 20m$ and $t_p = 2d$ to (d) S or (e) T calculated by perturbation (as the dots show) under heterogeneous parameters (Fig. 2(a)) or homogeneous parameters versus calculated by Fréchet kernels (as the lines show).

Different from Eq. (18) with a variable rate, $-i\omega G(x_Y)$ in Eq. (30) is a constant, so we can directly obtain the solution as:

$$M_S = \phi_G(x_o, \omega; x_Y) = -\frac{i\omega G(x_Y)}{2T}\sqrt{\frac{T}{i\omega S}}\left[exp\left(-\sqrt{\frac{i\omega S}{T}}|x_Y - x_o|\right) - exp\left(-\sqrt{\frac{i\omega S}{T}}|x_Y + x_o|\right)\right]$$

$$= -\frac{i\omega exp\left(-\sqrt{\frac{i\omega S}{T}}x_Y\right)}{2T}\sqrt{\frac{T}{i\omega S}}\left[exp\left(-\sqrt{\frac{i\omega S}{T}}|x_Y - x_o|\right) - exp\left(-\sqrt{\frac{i\omega S}{T}}|x_Y + x_o|\right)\right] \quad (33)$$

First, we think of the fundamental solution ϕ_{TG} of the equation is subjected to $\frac{\partial}{\partial x}\left[T\frac{\partial \phi_{TG}}{\partial x}\right] + \left[\frac{\partial \delta(x-x_Y)}{\partial x}\right] = i\omega S\phi_{TG}$. We can find that the solution of ϕ_{TG} is similar to ϕ_{TH}, i.e., the derivation similar to Eq. (26), so the solution of ϕ_{TG} can be easily obtained:

$$\phi_{TG} = \frac{\partial \phi_g}{\partial x} \quad (35)$$

Similarly, Eq. (34) describes a pumping test with a pumping well at x_Y and a complex pumping rate:

$$\left.\frac{\partial G}{\partial x}\right|_{x_Y} = H_s\sqrt{\frac{i\omega S}{T}}exp\left(-\sqrt{\frac{i\omega S}{T}}x_Y\right) \quad (36)$$

Similar to Eq. (33), we can directly obtain the solution as:

$$M_T = \phi_G(x_o, \omega; x_Y) = \begin{cases} \frac{H_s}{2T}\sqrt{\frac{i\omega S}{T}}exp\left(-\sqrt{\frac{i\omega S}{T}}x_Y\right)\left[exp\left(-\sqrt{\frac{i\omega S}{T}}|x_o - x_Y|\right) + exp\left(-\sqrt{\frac{i\omega S}{T}}|x_o + x_Y|\right)\right], & x_o > x_Y \\ \frac{H_s}{2T}\sqrt{\frac{i\omega S}{T}}exp\left(-\sqrt{\frac{i\omega S}{T}}x_Y\right)\left[-exp\left(-\sqrt{\frac{i\omega S}{T}}|x_o - x_Y|\right) + exp\left(-\sqrt{\frac{i\omega S}{T}}|x_o - x_Y|\right)\right], & x_o < x_Y \end{cases} \quad (37)$$

where M_S is the sensitivity of head response $G(x_o, t)$ on S, i.e., the Fréchet kernel of heterogeneous storativity on complex frequency response $G(x, \omega)$, which is also a complex number.

4.5. Sensitivity of G toT

Recalling Eq. (24), since the spatial derivative is involved as the "source term", we also examine the following governing equation with the source term inside the spatial derivative term:

$$\frac{\partial}{\partial x}\left[T\frac{\partial \phi_G}{\partial x}\right] + \left.\frac{\partial G}{\partial x}\right|_{x_Y}\left[\frac{\partial \delta(x - x_Y)}{\partial x}\right] = i\omega S\phi_G \quad (34)$$

where M_T is the sensitivity of head response $G(x_o, t)$ on T, i.e., the Fréchet kernel of heterogeneous transmissivity on complex frequency response $G(x, \omega)$, which is also a complex number.

4.6. Sensitivity of complex frequency response and their properties

The complex spatial sensitivity functions M_S and M_T (solutions in Eqs. (33) and (37)) contain both sensitivities of amplitude (A_G) and the phase shift (P_G) with respect to parameter Y. Assuming $G = a_G + b_G i$, the complex frequency response function of sensitivity $M_Y = a_Y + b_Y i$, according to Cauchy-Riemann condition, we can get:

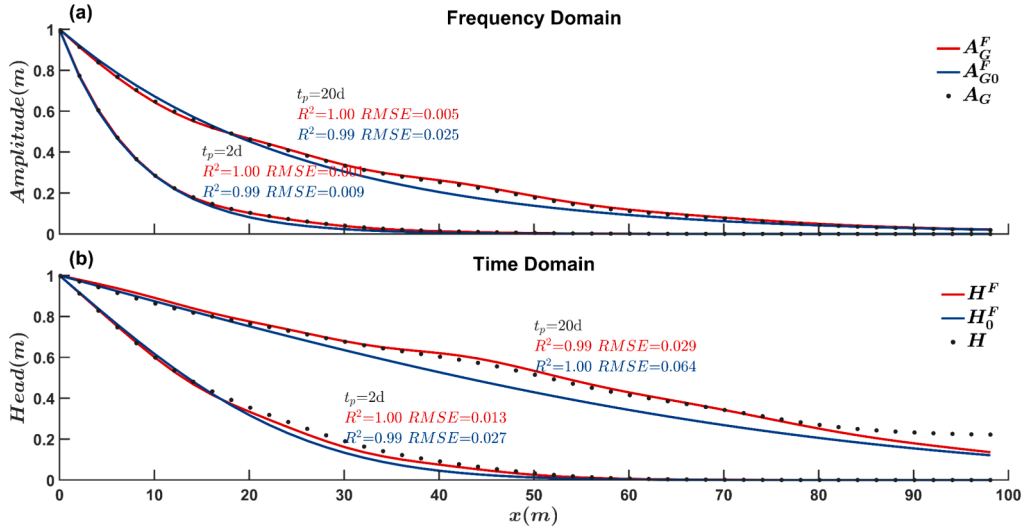

Fig. 3. (a) Amplitude calculated by Fréchet kernels A_G^F versus actual amplitude A_G in the heterogeneous aquifer and amplitude calculated in the aquifer with mean value T_0 and S_0, A_{G0}^F versus actual amplitude A_G in the heterogeneous aquifer under two periods $t_p = 2d$ and 20d. (b) Head calculated by Fréchet kernels H^F versus actual amplitude H in the heterogeneous aquifer and amplitude calculated in the aquifer with mean value T_0 and S_0, H_0^F versus actual amplitude H in the heterogeneous aquifer under two periods $t = 2d$ and 20d. Pearson correlation (R^2) and root-mean-square error ($RMSE$) are evaluation indexes.

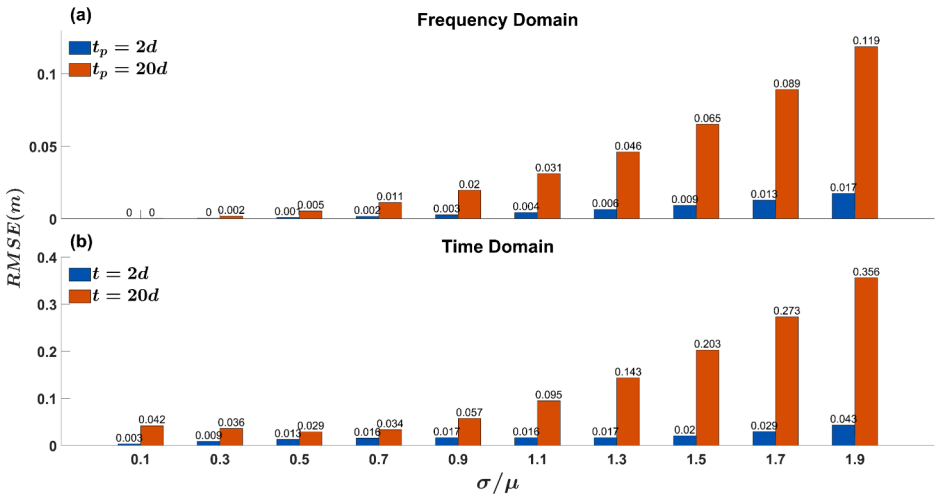

Fig. 4. (a) *RMSE* between amplitude calculated by Fréchet kernels A_G^F versus actual amplitude A_G in the heterogeneous aquifer under two periods $t_p = 2d$ and $20d$ under the different σ/μ of T and S normal distributions. (b) *RMSE* between head calculated by Fréchet kernels H^F versus actual head H in the heterogeneous aquifer under two times $t = 2d$ and $20d$ under the different σ/μ of T and S normal distributions.

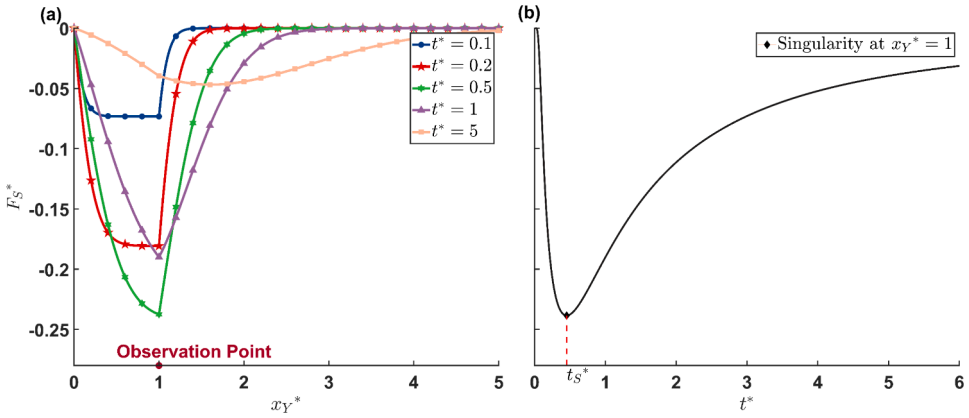

Fig. 5. (a) Dimensionless storativity kernel F_S^* for the dimensionless observation point at $x_o^* = 1$ for dimensionless times $t^* = 0.1$, 0.2, 0.5, 1, and 5; (b) the dimensionless storativity kernel reaches its minimum value at a time of $t_S^* \approx 0.45$ for the parameter location at $x_Y^* = 1$.

$$\frac{\partial A_G}{\partial Y} = \frac{\partial A_G}{\partial a_G} a_Y + \frac{\partial A_G}{\partial b_G} b_Y \tag{38}$$

$$\frac{\partial P_G}{\partial Y} = \frac{\partial P_G}{\partial a_G} a_Y + \frac{\partial P_G}{\partial b_G} b_Y \tag{39}$$

where $\frac{\partial A_G}{\partial a_G} = \frac{a_G}{A_G}$, $\frac{\partial A_G}{\partial b_G} = \frac{b_G}{A_G}$, $\frac{\partial P_G}{\partial a_G} = -\frac{b_G}{{A_G}^2}$, $\frac{\partial P_G}{\partial b_G} = \frac{a_G}{{A_G}^2}$, and $A_G = \sqrt{{a_G}^2 + {b_G}^2}$. An explicit form for the sensitivity of amplitude and phase shift is provided in Appendix B, where A_S [dimensionless], A_T [L^{-2} T], P_S [L^{-1}], and P_T [L^{-3} T] represent separately amplitude and phase shift Fréchet kernels to storativity and transmissivity.

5. Verification of Fréchet kernel

According to the meaning of Fréchet kernels, total sensitivities I_{tot} at x_o for the homogeneous aquifer in Section 3 is the spatial integral over the whole flow region of the corresponding Fréchet kernel:

$$I_{tot} = \int_0^{+\infty} F(x_o; x_Y) dx_Y \tag{40}$$

There is a significant difference in sensitivities for homogeneous and heterogeneous aquifers. For heterogeneous aquifers, sensitivities (Fréchet kernels) measure the responses at x_o to perturbations in $T(x_Y)$ or $S(x_Y)$ at the location of x_Y and are equal to spatial weighting functions with the variations of the parameters at specific location. For homogeneous aquifers, sensitivities refer to the responsiveness of a model's output or observation (such as hydraulic head, amplitude, and phase shift) to changes in model parameters across the entire domain of the aquifer.

Approaches to calculate sensitivities or head/amplitude in a heterogeneous aquifer by the Fréchet kernels are presented in this section, where the two cases prove the correctness of the Fréchet kernels as well as provide examples illustrating the application of the Fréchet kernels in heterogeneous aquifer scenarios.

5.1. Sensitivities calculated by perturbation versus Fréchet kernels

In this case, the resulting sensitivities of H and A_G by perturbation or Fréchet kernels (Eq. (10)) for the time domain (Fig. 2(b) and (c)) or the frequency domain (Fig. 2(d) and (e)) are shown, with T and S heterogeneity shown in Fig. 2(a) versus T and S homogeneity. Of course, under T and S heterogeneity, the two parameters satisfy the stationary assumption in geostatistical theory.

We find the lines calculated by Fréchet kernels coincide perfectly with the actual sensitives calculated by the perturbation method under T and S homogeneity, verifying the correctness of Fréchet kernels. Although the actual sensitives calculated by the perturbation method

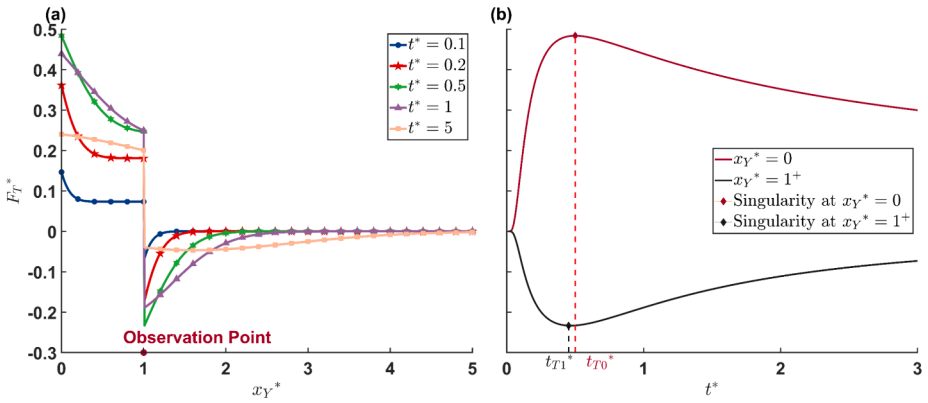

Fig. 6. (a) Dimensionless transmissivity kernel $F_T{}^*$ for the dimensionless observation point at $x_o^* = 1$ for dimensionless times $t^* = 0.1$, 0.2, 0.5, 1, and 5; (b) the dimensionless storativity kernels reach their minimum value at a time of $t_{T0}{}^* = 0.5$ and $t_{T1}{}^* \approx 0.45$ for the parameter location at $x_Y^* = 0$ and $x_Y^* = 1^+$.

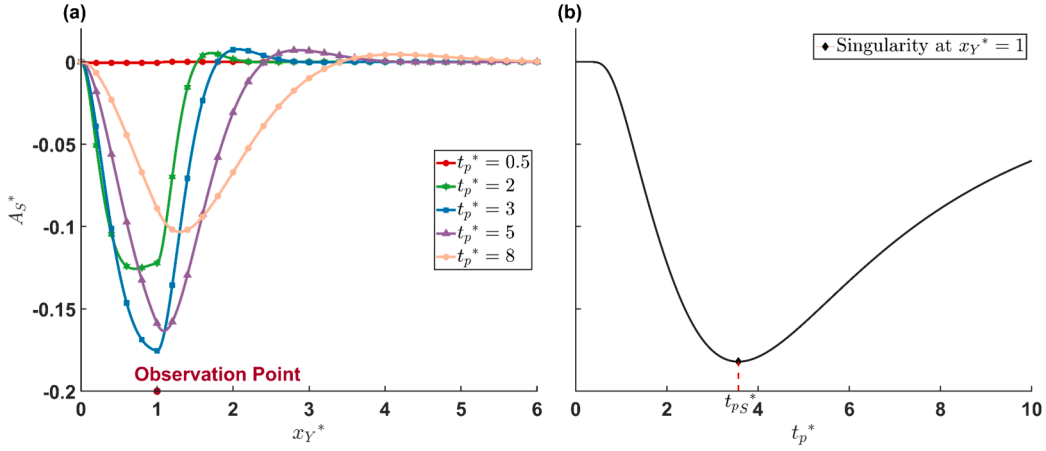

Fig. 7. (a) Dimensionless storativity kernel $A_S{}^*$ for the dimensionless observation point at $x_o^* = 1$ for dimensionless periods $t_p{}^* = 0.5$, 2, 3, 5, and 8; (b) the dimensionless storativity kernel reaches its minimum value at a dimensionless period of $t_{pS}{}^* \approx 3.57$ for the parameter location at $x_Y^* = 1$.

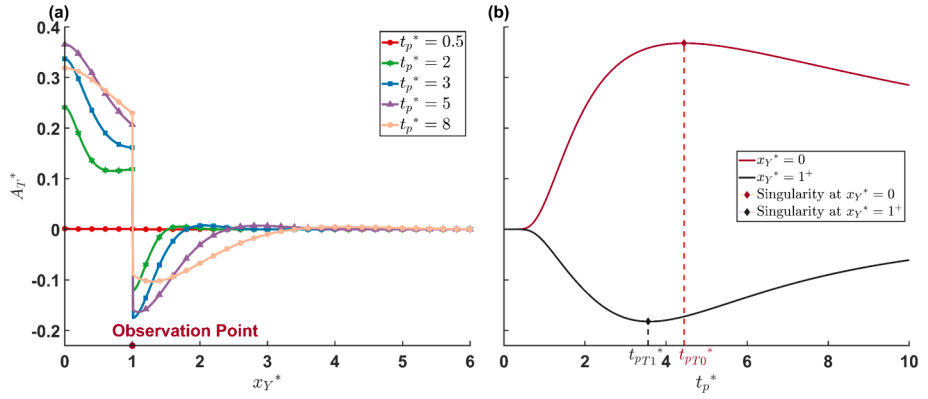

Fig. 8. (a) Dimensionless transmissivity kernel $A_T{}^*$ for the dimensionless observation point at $x_o^* = 1$ for dimensionless periods $t_p{}^* = 0.5$, 2, 3, 5, and 8; (b) the dimensionless transmissivity kernel reaches its minimum value at a dimensionless period of $t_{pT0}{}^* \approx 4.44$ and $t_{pT1}{}^* \approx 3.57$ for the parameter location at $x_Y^* = 0$ and $x_Y^* = 1$.

cannot coincide perfectly under T and S heterogeneity, this result may show that the Fréchet kernels can guide the calculation of sensitivity in the heterogeneous aquifer to some extent.

5.2. Relating Fréchet kernels to $\boldsymbol{H}$ or $\boldsymbol{A_G}$

In this case, according to Knight and Kluitenberg (2005) and Pechstein et al. (2015), we show through the Fréchet kernels as spatial weighting functions, the A_G and H in a specific heterogeneous aquifer can be calculated through the perturbation technique. Here, the parameter Y is defined as a spatial random function that can be split into a uniform mean Y_0, and a series of perturbations $\widetilde{Y}(x_Y)$. The head or amplitude at a particular location x_o in the heterogeneous aquifer is equal to the head or amplitude in the homogeneous aquifer, minus a

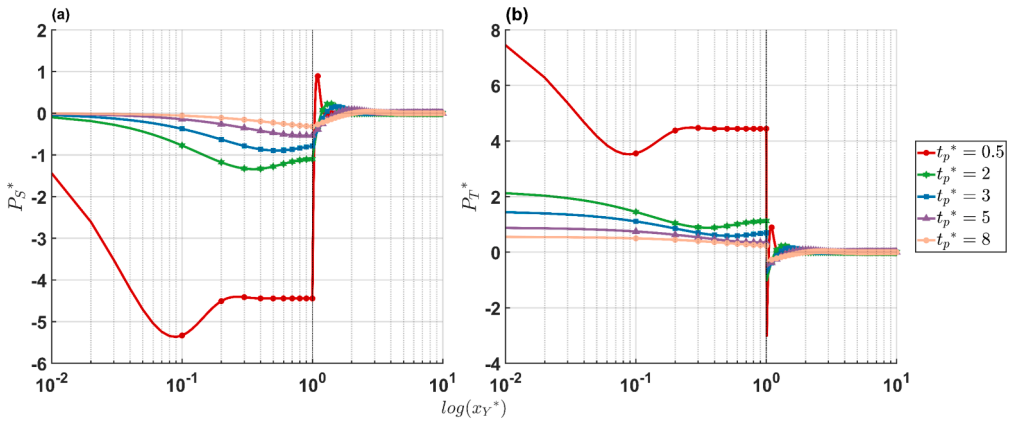

Fig. 9. (a) Dimensionless storativity kernel $P_S{}^*$ and (b) transmissivity kernel $P_T{}^*$ as a function of the logarithm of x_Y^* for the dimensionless observation point at $x_o^* = 10^0$ for dimensionless periods $t_p{}^* = 0.5$, 2, 3, 5, and 8.

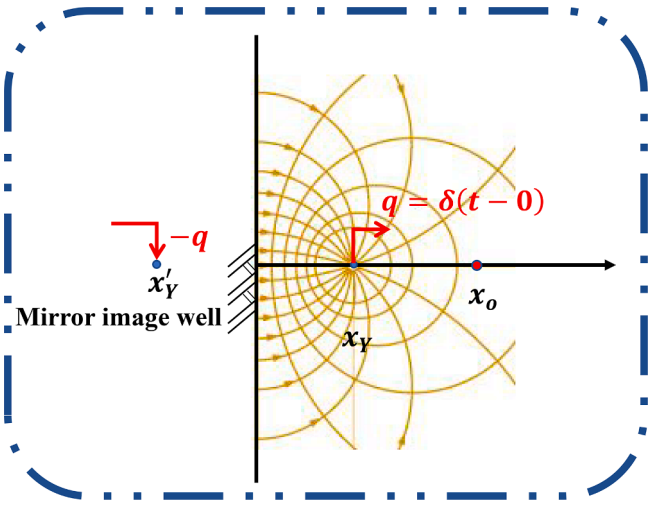

Fig. A1. Schematic of the solution by the method of image wells. For a pulse of flux q at x_Y, streamlines are shown as yellow lines and affect the sensitivity ϕ_0 of an observation position, x_o. To make $\phi_o(x,0) = 0$, an image well is located at the reflection of x_Y to simulate a no-flow boundary.

spatial convolution integral in terms of the transmissivity and storativity perturbations $\widetilde{Y}(x_Y)$, respectively. The Fréchet kernels F_T and F_S are spatial weighting functions of the perturbations of $\widetilde{T}(x_Y)$ and $\widetilde{S}(x_Y)$.

Suppose hydraulic parameter $Y(x)$ (e.g., $T(x)$ and $S(x)$) are functions of location x. $Y(x)$ can be viewed as uniform mean values Y_0 and a perturbation term $\widetilde{Y}(x)$, which can be expressed as

$$Y(x) = Y_0 + \widetilde{Y}(x) \tag{41}$$

The status variables $H^F(x_o,t)$ or $A_G^F(x_o,t)$ at a particular location x_o arising from $\widetilde{Y}(x)$ perturbations can be formulated as a convolution integral minus a uniform status variable as follows:

$$H^F(x_o,t) = H_0^F(x_o,t) - \int F_T(x_o,x_Y,t)\widetilde{T}(x_Y)dx_Y - \int F_S(x_o,x_Y,t)\widetilde{S}(x_Y)dx_Y \tag{42}$$

$$A_G^F(x_o,t) = A_{G0}^F(x_o,t) - \int A_T(x_o,x_Y,t)\widetilde{T}(x_Y)dx_Y - \int A_S(x_o,x_Y,t)\widetilde{S}(x_Y)dx_Y \tag{43}$$

with x_Y being the position vector of a particular anomaly in T, where H_0^F and A_{G0}^F are equal to the head or amplitude in the homogeneous aquifer with mean value T_0 and S_0 calculated by Eqs. (3) or (8), i.e., $H_0^F = H_s erfc\left(\frac{x\sqrt{S_0}}{2\sqrt{T_0 t}}\right)$ and $A_{G0}^F = H_s exp\left(-\sqrt{\frac{\omega S_0}{2T_0}}x\right)$. H_s represents the elevation of the river stage rise or amplitude at the boundary, where $H_s = 1m$ in this case.

The resulting head and amplitude under different times or periods are shown in Fig. 3(b) and (c), with T and S heterogeneity shown in Fig. 2(a). The state variables (H^F and A_G^F) obtained via Eqs. (42)–(43) are close to the real head (Fig. 3(b)) and amplitude (Fig. 3(c)) of the heterogeneous aquifer obtained directly by solving the groundwater flow equation. On the one hand, it can prove the correctness of Fréchet kernels; on the other hand, it provides examples illustrating the application of Fréchet kernels to heterogeneous aquifer scenarios.

Fig. 4 shows a specific case when the distributions of T and S satisfy $\sigma/\mu = 0.5$. By scaling the value of T and S in Fig. 2 (a), Fig. 4 compares the *RMSE* between A_G^F or H^F and actual A_G or H under different σ/μ values of normal distributions for frequency and time domains. With σ/μ (and hence variance) increasing, higher- order perturbation terms cannot be neglected and the Fréchet kernels based on the homogeneity hypothesis do not gradually apply.

6. Dimensionless versions of the Fréchet kernels and their properties

6.1. Case 1: Head response

According to Eq. (23), dimensionless versions of the storativity kernels for time response can be defined as:

$$F_S{}^*(x_o^*, t^*; x_Y^*) = \frac{x_o S}{H_s} F_S(x_o, t; x_Y) \tag{44}$$

Fig. 5(a) shows the behavior of the dimensionless storativity kernel $F_S{}^*$ as a function of x_Y^* at various dimensionless times t^*. It shows that for each t^*, the Fréchet kernel of S is always negative and its magnitude increases from zero at $x_Y^* = 0$ to a peak and then decreases to zero as x_Y^* increases. It reaches the highest negative peak value approximately at $t^* \approx 0.5$. Afterward, it decreases and the shape of $F_S{}^*$ broadens. As t^* increases, the position where $F_S{}^*$ reaches its maximum negative value deviates to the right of $x_Y^* = x_o^* = 1$, as shown by $t^* = 5$.

Physically, the negative value implies that if the observed head is higher than the head derived from the mean S values, the actual S values in the area between the river and the observation location must be smaller than the mean S value (Wang et al., 2017). Nevertheless, at late times, the kernel is spatially uniform over a large area including the boundary and observation point. The above result agrees with the dimensionless storativity kernel for a cross-hole pumping test in a 2-D,

unbounded aquifer along the direction joining the pumping and observation points (Knight and Kluitenberg, 2005). Furthermore, the shape of the negative area is not symmetrical about the midpoint between the observation point and the boundary due to the flow from the river to the observation location, which leads to the deviation of the late maximum position. In a pumping test in a 2-D domain studied by Sun et al. (2013), the shape is radially symmetrical about the midpoint.

At the observation point x_o^* (i.e., $x_Y^* = x_o^* = 1$), the time when the maximum negative value occurs can be derived by letting the time derivative of the Fréchet kernel equal to 0,

$$\frac{\partial F_S{}^*(x_o^*, t^*; 1)}{\partial t^*} = 0 \tag{45}$$

It can be shown mathematically that this is equivalent to

$$exp(-\frac{9}{4t_S{}^*})(9 - 2t_S{}^*) - exp\left(-\frac{1}{4t_S{}^*}\right)(1 - 2t_S{}^*) = 0 \tag{46}$$

The root of Eq. (46) is $t_S{}^* \approx 0.45$, which is the time when the maximum negative Fréchet value and singularity occurs (Knight and Kluitenberg, 2005).

Fig. 5(b) shows the behavior of $F_S{}^*$, at the location $x_Y^* = 1$, as a function of t^*. The magnitude of the kernel increases rapidly to a maximum negative value at a time of $t_S{}^*$ and then slowly decreases to zero.

The transmissivity kernels for time response can be defined as:

$$F_T{}^*(x_o^*, t^*; x_Y^*) = \frac{x_o T}{H_s} F_T(x_o, t; x_Y) \tag{47}$$

Fig. 6(a) displays the transmissivity kernel $F_T{}^*$ as a function of t^* at different x_Y^* values. Different from the sensitivity for S (Fig. 5(a)), its behavior exhibits a positive sensitivity zone before the observation location, and a negative zone after the location and a discontinuity exists at the location. The positive value inside the region $x_Y^* < x_o^*$ suggests that the T values in this region must be larger than the mean T if the observed head is higher than that based on the head calculated by the mean T and vice versa. On the other hand, if the head is higher than that based on the mean T, the T values in the negative region ($x_Y^* > x_o^*$) must be lower than the mean T.

The maximum positive kernel is at the boundary, while the maximum negative kernel is at the observation wells for all times (Fig. 6 (a)). Both the maximum values (either positive or negative) occur at a time of approximately $t^* \approx 0.5$. Unlike the cross-hole pumping test in a 2-D, unbounded aquifer, singularities at the pumping well come under infinite time (Knight and Kluitenberg, 2005; Leven and Dietrich, 2006). The difference is mainly induced by the difference of boundaries. The head variation is induced by the Dirichlet boundary in our case, but by the Neumann boundary (e.g., a constant pumping rate) for a pumping test problem. As a result, different flow fields lead to different sensitivity patterns.

At the boundary point $x_Y^* = 0$, and the observation well ($x_Y^* = 1^+$), the time when the maximum occurs can be found analytically by letting the time derivative of the Fréchet kernel equal to 0,

$$\frac{\partial F_T{}^*(x_o^*, t^*; 0)}{\partial t_{T0}{}^*} = 0 \quad \text{and} \quad \frac{\partial F_T{}^*(x_o^*, t^*; 1^+)}{\partial t_{T1}{}^*} = 0 \tag{48}$$

It can be shown mathematically that this is equivalent to

$$exp\left(-\frac{1}{4t_{T0}{}^*}\right)(1 - 2t_{T0}{}^*) = 0 \quad \text{and} \quad -exp\left(-\frac{1}{4t_{T1}{}^*}\right) + exp\left(-\frac{9}{4t_{T1}{}^*}\right) = 0 \tag{49}$$

The roots of Eq. (49) lead to $t_{T0}{}^* = 0.5$ and $t_{T1}{}^* \approx 0.45$. Fig. 6(b) shows the plot of $F_T{}^*$ at the locations of $x_Y^* = 0$ and $x_Y^* = 1^+$, varying with dimensionless times t^*. As in Fig. 6(b), the singularity at the boundary (near the maximum positive value) and observation wells (near the maximum negative on the right) occurs at a time of $t_{T0}{}^* = 0.5$ and $t_{T1}{}^* \approx 0.45$. The time corresponding to the negative singularity of the transmissivity kernel is the same as that of the storativity kernel, i.e., $t_{T1}{}^* = t_S{}^*$. And the time corresponding to the positive singularity at the boundary is the same as that of the sensitivity in the homogeneous aquifer (Section 3), i.e., $t_{To}{}^* = t_{tot}{}^* = 0.5$. The times of the occurrence of the negative and positive singularities of the transmissivity kernel are similar, i.e., there is not much difference between the values of $t_{T0}{}^*$ and $t_{T1}{}^*$.

6.2. Case 2: Amplitude for tidal response

In order to obtain a dimensionless kernel of amplitude and phase shift, dimensionless frequency ω^* is defined in Eq. (11):

$$\omega^* = \sqrt{\frac{\omega S}{T}} x_o \tag{50}$$

According to Eq. (B6) in Appendix B, dimensionless versions of the amplitude kernels for frequency response to storativity can be defined as:

$$A_S{}^*(x_o^*, \omega^*; x_Y^*) = \frac{x_o S}{H_s} A_S(x_o, t; x_Y) \tag{51}$$

To compare Fréchet kernels for the tidal fluctuations at different frequencies and the head at different times, we replace ω^* with the dimensionless period, $t_p{}^*$, among which $t_p{}^* = \frac{2\pi}{\omega^*}$ in Fig. 7(a). Similar to the shape of the kernel in time in Fig. 5(a), the periodic kernel is negative within the region, $x_Y^* < x_o^*$. However, different from the time kernel, the absolute sensitivity value along x_Y^* is not monotonic within the region, $x_Y^* < x_o^*$, as shown by $t_p{}^* = 1$ and 2. There are positive kernel values at $x_Y^* > x_o^*$. The explicit form of $A_S{}^*$ reveals a triangular function that renders the kernel values to become non-monotonic and oscillate positively and negatively, though the amplitudes in the homogeneous aquifer reveal a monotonic exponential attenuation (as shown in Eq. (9)). The positive value implies that if the observed amplitude is higher than the amplitude derived from the mean S values, the actual S values outside the observation location may be greater than the mean S value, which is different from the head Fréchet kernel in the time domain as shown in Fig. 5(a).

Similar to the time kernel, the period when the maximum negative value occurs is found through,

$$\frac{\partial A_S{}^*(x_o^*, \omega^*; 1)}{\partial \omega^*} = 0 \tag{52}$$

where, it can be shown mathematically that this is equivalent to

$$\begin{aligned}&\left(\omega^* - \sqrt{2}\right)exp\left(\sqrt{2}\,\omega^*\right) + \left(\sqrt{2} - 5\omega^*\right)sin\left(\sqrt{2}\,\omega^*\right)\\ &+ \left(\sqrt{2} - \omega^*\right)cos\left(\sqrt{2}\,\omega^*\right)\\ &= 0\end{aligned} \tag{53}$$

The root of Eq. (53) is given by $\omega^* \approx 1.76$ corresponding to $t_{pS}{}^* \approx 3.57$.

Fig. 7(b) shows the plot of $A_S{}^*$ at the location of $x_Y^* = 1$, as a function of the dimensionless period $t_p{}^*$. Compared to the time kernel in Fig. 5(b), at small periods, the kernel value is almost 0 and does not change with $t_p{}^*$ as dramatically as the time kernel. At high frequencies (e.g.,$t_p{}^* = 0.5$), the pressure wave dissipates quickly, and the wave cannot travel very far, resulting in a sensitivity of almost 0, as shown in Fig. 7(a).

According to Eq. (B7) in Appendix B, dimensionless transmissivity kernels for frequency response on amplitude can be defined as:

$$A_T{}^*(x_o^*, \omega^*; x_Y^*) = \frac{x_o T}{H_s} A_T(x_o, t; x_Y) \tag{54}$$

Its behavior is displayed in Fig. 8(a). Similar to the shape of the kernel in time in Fig. 6(a), the observation location divides the kernel's behavior into two distinct parts. For the region $x_Y^* < x_o^*$, the kernel is positive along x_Y^* and decreases non-monotonically as $t_p{}^*$ increases. In the region $x_Y^* > x_o^*$, the kernel is primarily negative at locations close to the observation point, then increases rapidly until it becomes slightly positive and decreases to zero at large distances. Consequently, a large amplitude of the observed response at the observation point would suggest a high T value within the $x_Y^* < x_o^*$ region or vice versa. On the other hand, in the region $x_Y^* > x_o^*$, where the kernel's values are negative, a large amplitude of the observed response at the observation point would suggest a low T value within the region. Beyond this negative region, the areas with small rises but diminishing positive humps may be positively correlated with the large amplitude at the observation point. However, the likelihood is small due to their small kernel values, thus they can be ignored.

The periods when the maximum values occur at $x_Y^* = 0$, and $x_Y^* = 1^+$ can be determined using

$$\frac{\partial A_T{}^*\left(x_o^*, \omega^*; 0\right)}{\partial \omega_{T0}{}^*} = 0 \text{ and } \frac{\partial A_T{}^*\left(x_o^*, \omega^*; 1^+\right)}{\partial \omega_{T1}{}^*} = 0 \tag{55}$$

That is,

$$exp\left(-\sqrt{\frac{1}{2}}\omega_{T0}{}^*\right)\left(\sqrt{2}\omega_{T0}{}^* - 2\right) = 0 \text{ and}$$

$$exp\left(\sqrt{2}\,\omega_{T1}{}^*\right)\left(\omega_{T1}{}^* - \sqrt{2}\right) + \left(\sqrt{2} - 5\omega_{T1}{}^*\right)sin\left(\sqrt{2}\omega_{TI}{}^*\right) + \left(\sqrt{2} - \omega_{T1}{}^*\right)cos\left(\sqrt{2}\,\omega_{T1}{}^*\right) = 0 \tag{56}$$

The roots of Eq. (56) are $\omega_{T0}{}^* = \sqrt{2}$ and $\omega_{T1}{}^* \approx 1.76$, corresponding to $t_{pT0}{}^* \approx 4.44$ and $t_{pT1}{}^* \approx 3.57$.

Fig. 8(b) shows the plot of $A_T{}^*$ as a function of t_p^* at two locations, $x_Y^* = 0$ and $x_Y^* = 1^+$. Compared to the time kernel varying with t^* in Fig. 6(b), the kernel value for amplitude to transmissivity does not change with $t_p{}^*$ as dramatically as the time kernel, indicating that the amplitude is not as sensitive to the T heterogeneity as the head in the case of a rise in river-stage. The period corresponding to the negative singularity of amplitude kernel to transmissivity is also the same as that of storativity kernel, i.e., $t_{pT1}{}^* = t_{pS}{}^*$ (Fig. 7(b)). And the period corresponding to the positive singularity of amplitude kernel to transmissivity is also the same as that of the sensitivity in the homogeneous aquifer (Section 3), i.e., $t_{pT0}{}^* = t_{p,tot}{}^* \approx 4.44$.

6.3. Case 2: Phase shift for tidal response

According to Appendix B and Eqs. (B8) and (B9), dimensionless versions of the storativity and transmissivity kernels for frequency response on phase shift can be defined as:

$$P_S{}^*(x_o^*, \omega^*; x_Y^*) = Sx_o P_S(x_o, t; x_Y) \tag{57}$$

$$P_T{}^*(x_o^*, \omega^*; x_Y^*) = Tx_o P_T(x_o, t; x_Y) \tag{58}$$

Fig. 9(a) and (b) show the behavior of the dimensionless storativity and transmissivity kernels $P_S{}^*(x_Y^*,\ t_p{}^*)$ and $P_T{}^*(x_Y^*,\ t_p{}^*)$ as a function of the logarithm of x_Y^*. We find that $P_S{}^*$ is negatively related to variations of S for $x_Y^* < x_o^*$, and alternates between positive and negative changes at the 0-valued point outside the x_o^*, which is the same as $A_S{}^*$. There are some differences from $A_S{}^*$. First, the $P_S{}^*$ kernel varies more drastically than $A_S{}^*$. Secondly, the $P_S{}^*$ kernel has a flat trend for $x_Y^* < x_o^*$ with $t_p{}^* \to \infty$. The shape of the $P_T{}^*$ kernel is the same as $A_T{}^*$, but the $P_T{}^*$ kernel varies more drastically and has an infinite peak around the point $x_Y^* = 0$ for $t_p{}^* \to \infty$.

7. Conclusions

The conclusions of this study are as follow:

(1) Previously, the explicit form of traditional Fréchet kernels in the time domain was limited to two-dimensional pumping test problems. This study is the first to derive Fréchet kernels for a 1-D semi-infinite aquifer, which is very important for characterizing aquifers under the influence of reservoir impoundment and river channels.
(2) Different from previous studies that provided an explicit form for Fréchet kernels in the time domain, we derive the Fréchet kernels in the frequency domain to solve for the sensitivity of periodic head characteristics (amplitude or phase shift) to parameters. This result is of great significance and practical use for characterizing aquifers under the influence of tides.
(3) The hydraulic head or amplitude Fréchet kernels to S or T in the case of river stage rise and tidal variation have common features: similar spatial patterns for S or T over time or period. For S, the Fréchet kernels start from 0 at the boundaries, then become negative continuously to the observation point. For T, the observation location divides the kernels into two regions of negative and positive sensitivity values, and a discontinuity exists at the observation location. This means that the joint estimation of spatially distributed T and S based on head/amplitude observations alone can be challenging because both T and S influence the observations, yet their effects can be difficult to disentangle.
(4) Based on the analysis of the temporal/periodic Fréchet kernels between head/amplitude observed at an observation location and T and S everywhere in the aquifer, we recommend an optimal dimensionless time ($t_{T1}{}^* = t_S{}^*$) or period ($t_{pT1}{}^* = t_{pS}{}^*$) that the observations are the highest value for use in parameter estimation (i.e., observation location and boundary).
(5) Although Fréchet kernels of amplitude and head have similar spatial patterns for S or T over time or period, there is difference for head or amplitude data to characterize the spatial distributions of hydraulic parameters. The amplitudes in a homogeneous aquifer show a monotonic exponential attenuation, Fréchet kernels show positive and negative variations behind the observation point, a property that Fréchet kernels of head response do not have.
(6) Joint interpretation of multi-time or multi-frequency data can be more instrumental than single observation in hydrogeological parameter inversion because multi-frequency or multi-time Fréchet kernels can yield different characteristics of head or fluctuation responses to parameter perturbations.

Although the limitation of this study is that the derivation is based on the stationary assumption in geostatistical theory and small variance, the analytical solutions for Fréchet kernels for hydraulic head and tidal responses can be generalized to hydrologic or geophysical inversion and help guide the monitoring well network design. Moreover, the analytical solution is expressed as explicit functions without a convolution integration, which can be easily applicable to interpret and estimate spatially averaged parameters as spatial weighting functions.

CRediT authorship contribution statement

Jiong Zhu: Writing – original draft, Visualization, Validation, Methodology, Conceptualization. **Yuanyuan Zha:** Writing – review & editing, Supervision, Conceptualization. **Tian-Chyi Jim Yeh:** . **Walter A. Illman:** Writing – review & editing.

Declaration of competing interest

The authors declare that they have no known competing financial interests or personal relationships that could have appeared to influence the work reported in this paper.

Data availability

Data will be made available on request.

Acknowledgments

This study is supported by the National Natural Science Foundation of China (Grant No. 52279042), the Key Research and Developement Program in Guanxi (AB23026021), and the Open Research Fund of Guangxi Key Laboratory of Water Engineering Materials and Structures, the Guangxi Institute of Water Resources Research (GXHRI-WEMS-2022-07). Walter A. Illman appreciates the support of the Discovery Grant from the Natural Sciences and Engineering Research Council of Canada (NSERC) and the support of "The Belt and Road" Exchange Innovative Foreign Experts (G2023153008L) from the Ministry of Science and Technology of China, which made this collaboration possible. This work benefitted from insightful and detailed comments from anonymous reviewers and the editors.

Appendix A. Derivation of the fundamental solution

The solution to Eq. (19) takes a form similar to the derivative of Eq. (1) with respect to t, but there are differences in the boundary conditions between these two equations ($H(0,0) = H_s$ in Eq. (1), but $\phi_0(0,0) = 0$ in Eq. (19)).

The fundamental solution without considering the initial condition, boundary conditions, and source term is:

$$\phi_{0,general} = -C_H \frac{\sqrt{D}}{\sqrt{\pi}} exp\left(\frac{-(x-x_Y)^2}{4Dt}\right) t^{-1/2} \tag{A1}$$

where C_H is defined by the boundary conditions for a semi-infinite domain. Eq. (A1) is equivalent to taking the partial derivative of Eq. (4) with respect to t, in order to solve the Dirac delta function, $\delta(t-0)$ in Eq. (19) (Zha et al., 2020). $\delta(x-x_Y)$ can be regarded as an inner discontinuous flux condition and can be written as (Gunduz and Aral, 2005):

$$T\frac{\partial \phi_{0,general}}{\partial x}\bigg|_{x_Y^-} - T\frac{\partial \phi_{0,general}}{\partial x}\bigg|_{x_Y^+} = \delta(t-0) \tag{A2}$$

Integrating both sides of this equation and Eq. (19) with respect to t, and making $\int \phi_{0,general} dt = C_H \frac{2\sqrt{Dt}}{T} ierfc\left(\frac{1}{2\sqrt{Dt}}|x-x_Y|\right)$, Eq. (A2) can be written as:

$$T\frac{\partial \int \phi_{0,general} dt}{\partial x}\bigg|_{x_Y^-} - T\frac{\partial \int \phi_{0,general} dt}{\partial x}\bigg|_{x_Y^+} = 1 \tag{A3}$$

According to Eq. (A3), we get $C_H = \frac{1}{2T}$.

Now, $\phi_{0,general} = -\frac{1}{2T}\frac{\sqrt{D}}{\sqrt{\pi}} exp\left(\frac{-(x-x_Y)^2}{4Dt}\right) t^{-1/2}$ can satisfy Eq. (19). To make it satisfy the boundary condition (i.e., $\phi_0(0,0) = 0$), we adopt a method based on modified image wells in which the flow moving toward (or away from) the boundary is modified by its current image well to simulate a no-flow boundary (Fig. A1) (Moon and Fernandez, 2010; Sridharan and Hein, 2019; Zhou et al., 2022). Assuming to be implicit in the spatial density structure is the image source corresponding to the type of boundary condition at x_Y, with flux $q = -\delta(t-0)$.

According to the method of image wells, in its most general form, the fundamental solution of Eq. (19) with boundary condition (Eqs. (15.a) and (15.b)) with ϕ_H replaced by ϕ_0) for the sensitivity is:

$$\phi_0 = -\frac{1}{2T}\frac{\sqrt{D}}{\sqrt{\pi}}[exp(-\frac{|x_Y-x|^2}{4Dt})t^{-1/2} - exp(-\frac{|x_Y+x|^2}{4Dt})t^{-1/2}] \tag{A4}$$

Appendix B. Fréchet kernels of the amplitude and the phase shift

The complex frequency response functions M_S and M_T (solutions in Eqs. (33) and (37)) contain both sensitivities of amplitude (A_G) and the phase shift (P_G) with respect to the parameter Y (i.e., S and T). Next, we derive the Fréchet kernels of the amplitude and the phase shift for S.

Recalling Eq. (33), for $x_Y < x_o$, it can be written as:

$$M_S = -\frac{H_s}{2S}\sqrt{\frac{\omega S}{T}} exp\left(\frac{\pi}{4}i\right)\left[exp\left(-\sqrt{\frac{\omega S}{2T}}(i+1)(x_o)\right) - exp\left(-\sqrt{\frac{\omega S}{2T}}(i+1)(x_o+2x_Y)\right)\right] \tag{B1}$$

For the complex frequency response functions M_S, considering its real parts $Re(.)$ and imaginary parts $Im(.)$ separately, we can get:

$a_Y = Re(M_S)$

$$= -\frac{H_s}{2S}\sqrt{\frac{\omega S}{T}} exp\left(-\sqrt{\frac{\omega S}{2T}}x_o\right) cos\left(\frac{\pi}{4} - \sqrt{\frac{\omega S}{2T}}x_o\right) + \frac{H_s}{2S}\sqrt{\frac{\omega S}{T}} exp\left(-\sqrt{\frac{\omega S}{2T}}(x_o+2x_Y)\right) cos\left(\frac{\pi}{4} - \sqrt{\frac{\omega S}{2T}}(x_o+2x_Y)\right) \tag{B2.a}$$

$b_Y = Im(M_S)$

$$= -\frac{H_s}{2S}\sqrt{\frac{\omega S}{T}}exp\left(-\sqrt{\frac{\omega S}{2T}}x_o\right)sin\left(\frac{\pi}{4}-\sqrt{\frac{\omega S}{2T}}x_o\right)+\frac{H_s}{2S}\sqrt{\frac{\omega S}{T}}exp\left(-\sqrt{\frac{\omega S}{2T}}(x_o+2x_Y)\right)sin\left(\frac{\pi}{4}-\sqrt{\frac{\omega S}{2T}}(x_o+2x_Y)\right) \tag{B2.b}$$

For the complex frequency response function, G at the location x_o, according to Eq. (8), we can get its amplitude ($A_G = H_s exp(-ax_o)$), and considering its real and imaginary parts separately, we obtain:

$$a_G = H_s exp\left(-\sqrt{\frac{\omega S}{2T}}x_o\right)cos\left(-\sqrt{\frac{\omega S}{2T}}x_o\right) \tag{B3.a}$$

$$b_G = H_s exp\left(-\sqrt{\frac{\omega S}{2T}}x_o\right)sin\left(-\sqrt{\frac{\omega S}{2T}}x_o\right) \tag{B3.b}$$

According to Eq. (38), the Fréchet kernels of the amplitude (A_S) to S can be directly derived for $x_Y < x_o$:

$$A_S = \frac{Re(M_S)a_G + Im(M_S)b_G}{A_G}$$

$$= -\frac{H_s}{2S}\sqrt{\frac{\omega S}{T}}exp\left(-\sqrt{\frac{\omega S}{2T}}x_o\right)cos\left(\frac{\pi}{4}\right)+\frac{H_s}{2S}\sqrt{\frac{\omega S}{T}}exp\left(-\sqrt{\frac{\omega S}{2T}}(x_o+2x_Y)\right)cos\left(\frac{\pi}{4}-\sqrt{\frac{2\omega S}{T}}x_Y\right),\ x_Y < x_o \tag{B4}$$

and, the Fréchet kernel of the phase shift (P_S) to S is (Eq. (39)):

$$P_S = \frac{-Re(M_S)a_G + Im(M_S)b_G}{(A_G)^2}$$

$$= -\frac{1}{2S}\sqrt{\frac{\omega S}{T}}sin\left(\frac{\pi}{4}\right)+\frac{1}{2S}\sqrt{\frac{\omega S}{T}}exp\left(-\sqrt{\frac{2\omega S}{T}}x_Y\right)sin\left(\frac{\pi}{4}-\sqrt{\frac{2\omega S}{T}}x_Y\right),\ x_Y < x_o \tag{B5}$$

Similar to the above derivation, we can derive the Fréchet kernels of amplitude and the phase shift with respect to S and T, i.e., A_S, P_S, A_T, and P_T.

$$A_S = \begin{cases} -\frac{H_s}{2S}\sqrt{\frac{\omega S}{T}}exp\left(-\sqrt{\frac{\omega S}{2T}}x_o\right)cos\left(\frac{\pi}{4}\right)+\frac{H_s}{2S}\sqrt{\frac{\omega S}{T}}exp\left(-\sqrt{\frac{\omega S}{2T}}(x_o+2x_Y)\right)cos\left(\frac{\pi}{4}-\sqrt{\frac{2\omega S}{T}}x_Y\right), & x_Y < x_o \\ -\frac{H_s}{2S}\sqrt{\frac{\omega S}{T}}exp\left(-\sqrt{\frac{\omega S}{2T}}(2x_Y-x_o)\right)cos\left(\frac{\pi}{4}-\sqrt{\frac{2\omega S}{T}}(x_Y-x_o)\right)+\frac{H_s}{2S}\sqrt{\frac{\omega S}{T}}exp\left(-\sqrt{\frac{\omega S}{2T}}(x_o+2x_Y)\right)cos\left(\frac{\pi}{4}-\sqrt{\frac{2\omega S}{T}}x_Y\right), & x_Y > x_o \end{cases} \tag{B6}$$

$$P_S = \begin{cases} -\frac{1}{2S}\sqrt{\frac{\omega S}{T}}sin\left(\frac{\pi}{4}\right)+\frac{1}{2S}\sqrt{\frac{\omega S}{T}}exp\left(-\sqrt{\frac{2\omega S}{T}}x_Y\right)sin\left(\frac{\pi}{4}-\sqrt{\frac{2\omega S}{T}}x_Y\right), & x_Y < x_o \\ -\frac{1}{2S}\sqrt{\frac{\omega S}{T}}\sqrt{\frac{\omega S}{T}}exp\left(-\sqrt{\frac{2\omega S}{T}}(x_Y-x_o)\right)sin\left(\frac{\pi}{4}-\sqrt{2}\,\omega^*\left(x_Y^*-1\right)\right)+\frac{1}{2S}\sqrt{\frac{\omega S}{T}}exp\left(-\sqrt{\frac{2\omega S}{T}}x_Y\right)sin\left(\frac{\pi}{4}-\sqrt{\frac{2\omega S}{T}}x_Y\right), & x_Y > x_o \end{cases} \tag{B7}$$

$$A_T = \begin{cases} \frac{H_s}{2T}\sqrt{\frac{\omega S}{T}}exp\left(-\sqrt{\frac{\omega S}{2T}}x_o\right)cos\left(\frac{\pi}{4}\right)+\frac{H_s}{2T}\sqrt{\frac{\omega S}{T}}exp\left(-\sqrt{\frac{\omega S}{2T}}(x_o+2x_Y)\right)cos\left(\frac{\pi}{4}-\sqrt{\frac{2\omega S}{T}}x_Y\right), & x_Y < x_o \\ -\frac{H_s}{2T}\sqrt{\frac{\omega S}{T}}exp\left(-\sqrt{\frac{\omega S}{2T}}(2x_Y-x_o)\right)cos\left(\frac{\pi}{4}-\sqrt{\frac{2\omega S}{T}}(x_Y-x_o)\right)+\frac{H_s}{2T}\sqrt{\frac{\omega S}{T}}exp\left(-\sqrt{\frac{\omega S}{2T}}(x_o+2x_Y)\right)cos\left(\frac{\pi}{4}-\sqrt{\frac{2\omega S}{T}}x_Y\right), & x_Y > x_o \end{cases} \tag{B8}$$

$$P_T = \begin{cases} \frac{1}{2T}\sqrt{\frac{\omega S}{T}}sin\left(\frac{\pi}{4}\right)+\frac{1}{2T}\sqrt{\frac{\omega S}{T}}exp\left(-\sqrt{\frac{2\omega S}{T}}x_Y\right)sin\left(\frac{\pi}{4}-\sqrt{\frac{2\omega S}{T}}x_Y\right), & x_Y < x_o \\ -\frac{1}{2T}\sqrt{\frac{\omega S}{T}}exp\left(-\sqrt{\frac{2\omega S}{T}}(x_Y-x_o)\right)sin\left(\frac{\pi}{4}-\sqrt{\frac{2\omega S}{T}}(x_Y-x_o)\right)+\frac{1}{2T}\sqrt{\frac{\omega S}{T}}exp\left(-\sqrt{\frac{2\omega S}{T}}x_Y\right)sin\left(\frac{\pi}{4}-\sqrt{\frac{2\omega S}{T}}x_Y\right), & x_Y > x_o \end{cases} \tag{B9}$$

References

Carrera, J., Neuman, S.P., 1986. Estimation of aquifer parameters under transient and steady state conditions:1. Maximum likelihood method incorporating prior information. Water Resour. Res. 22 (2), 199–210.

Castagna, M., Becker, M.W., Bellin, A., 2011. Joint estimation of transmissivity and storativity in a bedrock fracture. Water Resour. Res. 47 (9).

Clifton, P.M., Neuman, H.P., 1982. Effects of kriging and inverse modeling on conditional simulation of the Avra Valley aquifer in southern Arizona. Water Resour. Res. 18 (4), 1215–1234.

Copty, N.K., Trinchero, P., Sanchez-Vila, X., 2011. Inferring spatial distribution of the radially integrated transmissivity from pumping tests in heterogeneous confined aquifers. Water Resour. Res. 47 (5), 1–11. https://doi.org/10.1029/2010WR009877.

Dagan, G., 1982a. Stochastic modeling of groundwater flow by unconditional and conditional probabilities 1. Conditional simulation and the direct problem. Water Resour. Res. 18 (4), 813–833.

Dagan, G., 1982b. Stochastic modeling of groundwater flow by unconditional and conditional probabilities 2. The Solute Transport. *Water Resources Research* 18 (4), 835–848.

Erskine, A.D., 1991. The effect of tidal fluctuation on a coastal aquifer in the UK. Groundwater.

Fischer, P., Jardani, A., Krimissa, M., Couegnas, C., 2020. Hydraulic characterization of a highly anthropized coastal aquifer subject to tidal fluctuations. Hydrgeol. J. 28 (7), 2559–2571. https://doi.org/10.1007/s10040-020-02215-w.
Gunduz, O., Aral, M.M., 2005. A dirac-δ function notation for source/sink terms in groundwater flow. J. Hydrol. Eng. 10 (5), 420–427. https://doi.org/10.1061/(asce)1084-0699(2005)10:5(420).
Guo, H., Jiao, J.J., Li, H., 2010. Groundwater response to tidal fluctuation in a two-zone aquifer. J. Hydrol. 381 (3–4), 364–371. https://doi.org/10.1016/j.jhydrol.2009.12.009.
Guo, Q., Li, H., Boufadel, M.C., Xia, Y., Li, G., 2007. Tide-induced groundwater head fluctuation in coastal multi-layered aquifer systems with a submarine outlet-capping. Adv. Water Resour. 30 (8), 1746–1755. https://doi.org/10.1016/j.advwatres.2007.01.003.
Huang, Y., Yeh, H., 2007. The use of sensitivity analysis in on-line aquifer parameter estimation. J. Hydrol. 335, 406–418. https://doi.org/10.1016/j.jhydrol.2006.12.007.
Hwang, H.S., Hamm, S.Y., Cheong, J.Y., Lee, S.H., Ha, K., Lee, C., Woo, N.C., Yun, S.M., Kim, K.H., 2020. Effective time- and frequency-domain techniques for interpreting seismic precursors in groundwater level fluctuations on Jeju Island. Korea. *Scientific Reports* 10 (1), 1–14. https://doi.org/10.1038/s41598-020-64586-0.
Johnson, T.C., Slater, L.D., Ntarlagiannis, D., Day-Lewis, F.D., Elwaseif, M., 2012. Monitoring groundwater-surface water interaction using time-series and time-frequency analysis of transient three-dimensional electrical resistivity changes. Water Resour. Res. 48 (7), 1–13. https://doi.org/10.1029/2012WR011893.
Kitanidis, P.K., 1995. Quasi-linear geostatistical theory for inversing. Water Resour. Res. 31 (10), 2411–2419.
Kitanidis, P.K., Vomvoris, E.G., 1983. A Geostatistical Approach to the Inverse Problem In Groundwater Modeling (Steady State) and One-Dimensional Simulations. Water Resour. Res. 19 (3), 677–690.
Knight, J.H., Kluitenberg, G.J., 2005. Some analytical solutions for sensitivity of well tests to variations in storativity and transmissivity. Adv. Water Resour. 28 (10 SPEC. ISS.), 1057–1075. https://doi.org/10.1016/j.advwatres.2004.08.018.
Leven, C., Dietrich, P., 2006. What information can we get from pumping tests? Comparing pumping test configurations using sensitivity coefficients. J. Hydrol. 319 (1–4), 199–215. https://doi.org/10.1016/j.jhydrol.2005.06.030.
Li, H., Jiao, J.J., Tang, Z., 2006. Semi-numerical simulation of groundwater flow induced by periodic forcing with a case-study at an island aquifer. J. Hydrol. 327 (3–4), 438–446. https://doi.org/10.1016/j.jhydrol.2005.11.032.
Lu, Z., Vesselinov, V.V., 2015. Analytical sensitivity analysis of transient groundwater flow in a bounded model domain using the adjoint method. Water Resour. Res. 51 (7), 5060–5080.
Manewell, N., Doherty, J., Hayes, P., 2023. Spatial averaging implied in aquifer test interpretation: The meaning of estimated hydraulic properties. Front. Earth Sci. 10 (January), 1–18. https://doi.org/10.3389/feart.2022.1079287.
Mao, D., Yeh, T.C.J., Wan, L., Wen, J.C., Lu, W., Lee, C.H., Hsu, K., 2013. Joint interpretation of sequential pumping tests in unconfined aquifers. Water Resour. Res. 49 (4), 1782–1796. https://doi.org/10.1002/wrcr.20129.
Mazzilli, N., Guinot, V., Jourde, H., 2010. Sensitivity analysis of two-dimensional steady-state aquifer flow equations. Implications for groundwater flow model calibration and validation. Adv. Water Resour. 33 (8), 905–922. https://doi.org/10.1016/j.advwatres.2010.04.014.
Mclaughlin, D., Parsons, R.M., Townley, L.R., 1996. A reassessment of the groundwater inverse problem. Water Resour. Res. 32 (5), 1131–1161.
Mohri, K., Hibiya, T., Iwamae, N., 2010. Revisiting internal wave generation by tide-topography interaction. J. Geophys. Res. Oceans 115 (11), 1–9. https://doi.org/10.1029/2009JC005908.
Moon, J., Fernandez, G., 2010. Effect of excavation-induced groundwater level drawdown on tunnel in flow in a jointed rock mass. Eng. Geol. 110 (3–4), 33–42. https://doi.org/10.1016/j.enggeo.2009.09.002.
Oliver, D.S., 1993. The influence of nonuniform transmissivity and storativity on drawdown. Water Resour. Res. 29 (1).
Pechstein, A., Attinger, S., Krieg, R., Copty, K., 2015. Estimating transmissivity from single-well pumping tests in heterogeneous aquifers. Water Resour. Res. 5 (3), 2. https://doi.org/10.1111/j.1752-1688.1969.tb04897.x.
Pouladi, B., Linde, N., Longuevergne, L., Bour, O., 2021. Individual and joint inversion of head and flux data by geostatistical hydraulic tomography. Adv. Water Resour. 154, 103960 https://doi.org/10.1016/j.advwatres.2021.103960.
Qi, Z., Shi, Z., Rasmussen, T.C., 2022. Time- and frequency-domain determination of aquifer hydraulic properties using water-level responses to natural perturbations: A case study of the Rongchang Well, Chongqing, southwestern China. J. Hydrol. 128820 https://doi.org/10.1016/j.jhydrol.2022.128820.
Rowe, P.P., 1960. An equation for estimating transmissibility and coefficient of storage from river-level fluctuations. J. Geophys. Res. 65 (10).
Shuai, P., Knappett, P.S.K., Hossain, S., Hosain, A., Rhodes, K., Ahmed, K.M., Cardenas, M.B., 2017. The impact of the degree of aquifer confinement and anisotropy on tidal pulse propagation. Groundwater 55 (4), 519–531. https://doi.org/10.1111/gwat.12509.
Slooten, L.J., Carrera, J., Castro, E., Fernandez-Garcia, D., 2010. A sensitivity analysis of tide-induced head fluctuations in coastal aquifers. J. Hydrol. 393 (3–4), 370–380. https://doi.org/10.1016/j.jhydrol.2010.08.032.
Sobolevskaia, V., Cardenas, M.B., Hasanov, A.K., Knappett, P.S.K., 2021. Aquifer diffusivity estimation through joint inversion of the amplitude ratios and time lags of dominant frequencies of fluctuating head. Water Resour. Res. 57 (6), 1–12. https://doi.org/10.1029/2020WR027912.
Sridharan, V.K., Hein, A.M., 2019. Analytical solution of advection-dispersion boundary value processes in environmental flows. Water Resour. Res. 55 (12), 10130–10143. https://doi.org/10.1029/2019WR025429.
Sun, R., Yeh, T.C.J., Mao, D., Jin, M., Lu, W., Hao, Y., 2013. A temporal sampling strategy for hydraulic tomography analysis. Water Resour. Res. 49 (7), 3881–3896. https://doi.org/10.1002/wrcr.20337.
Trefry, M.G., 1999. Periodic forcing in composite aquifers. Adv. Water Resour. 22 (6), 645–656. https://doi.org/10.1016/S0309-1708(98)00037-2.
Trefry, M.G., Bekele, E., 2004. Structural characterization of an island aquifer via tidal methods. Water Resour. Res. 40 (1), 1–21. https://doi.org/10.1029/2003WR002003.
Trefry, M.G., Johnton, C.D., 1998. Pumping Test Analysis for a Tidally Forced Aquifer. Groundwater 36 (3).
Trefry, M.G., McLaughlin, D., Lester, D.R., Metcalfe, G., Johnston, C.D., Ord, A., 2011. Stochastic relationships for periodic responses in randomly heterogeneous aquifers. Water Resour. Res. 47 (8), 1–18. https://doi.org/10.1029/2011WR010444.
Vandenbohede, A., Lebbe, L., 2007. Effects of tides on a sloping shore: Groundwater dynamics and propagation of the tidal wave. Hydrgeol. J. 15 (4), 645–658. https://doi.org/10.1007/s10040-006-0128-y.
Wang, Y.L., Yeh, T.C.J., Wen, J.C., Huang, S.Y., Zha, Y., Tsai, J.P., Hao, Y., Liang, Y., 2017. Characterizing subsurface hydraulic heterogeneity of alluvial fan using riverstage fluctuations. J. Hydrol. 547, 650–663. https://doi.org/10.1016/j.jhydrol.2017.02.032.
Wang, Y.L., Yeh, T.C.J., Wen, J.C., Gao, X., Zhang, Z., Huang, S.Y., 2019. Resolution and Ergodicity Issues of River Stage Tomography With Different Excitations. Water Resour. Res. 55 (6), 4974–4993. https://doi.org/10.1029/2018WR023204.
Welch, C., Cook, P.G., Harrington, G.A., Robinson, N.I., 2013. Propagation of solutes and pressure into aquifers following river stage rise. Water Resour. Res. 49 (9), 5246–5259. https://doi.org/10.1002/wrcr.20408.
Xia, R., Liang, Y., Jim Yeh, T.C.J., Dang, X., Gu, X., Xu, B., 2023. Characterizing hydraulic heterogeneity of Bayin River Basin using river stage tomography. J. Hydrol. 621 (March), 129547 https://doi.org/10.1016/j.jhydrol.2023.129547.
Yeh, W.W., 1986. Review of parameter identification procedures in groundwater hydrology: The inverse problem. Water Resour. Res. 22 (2), 95–108.
Yeh, T.C.J., Liu, S., 2000. Hydraulic tomography: Development of a new aquifer test method. Water Resour. Res. 36 (8), 2095–2105. https://doi.org/10.1029/2000WR900114.
Zha, Y., Yeh, T.C.J., Mao, D., Yang, J., Lu, W., 2014. Usefulness of flux measurements during hydraulic tomographic survey for mapping hydraulic conductivity distribution in a fractured medium. Adv. Water Resour. 71, 162–176. https://doi.org/10.1016/j.advwatres.2014.06.008.
Zha, Y., Shi, L., Liang, Y., Michael Tso, C.H., Zeng, W., Zhang, Y., 2020. Analytical sensitivity map of head observations on heterogeneous hydraulic parameters via the sensitivity equation method. J. Hydrol. 591 (July), 125282 https://doi.org/10.1016/j.jhydrol.2020.125282.
Zhang, H., 2021. Characterization of a multi-layer karst aquifer through analysis of tidal fluctuation. J. Hydrol. 601 (July), 126677 https://doi.org/10.1016/j.jhydrol.2021.126677.
Zhao, Z., Illman, W.A., 2021. On the importance of considering specific storage heterogeneity in hydraulic tomography: Laboratory sandbox and synthetic studies. J. Hydrol. 593, 125874.
Zhou, Y., Zheng, Z., Zhao, G., 2022. Analytical models for heat transfer around a single ground heat exchanger in the presence of both horizontal and vertical groundwater fl ow considering a convective boundary condition. Energy 245, 123159. https://doi.org/10.1016/j.energy.2022.123159.